NRIAG JOURNAL OF ASTRONOMY AND GEOPHYSICS
2025, VOL. 14, NO. 1, 1–22
https://doi.org/10.1080/20909977.2025.2450751

Gas saturation and tuning effect investigations in high seismic amplitude anomalies: a case study of the "Taadoy" field in Nigeria

L. Adeoti, O.J. Allo, T. Oyeniran, O.Y. Adeogun, G. Anukwu and J.T. Adegbite

Department of Geosciences, Faculty of Science, University of Lagos, Lagos, Nigeria

ABSTRACT

The assumption that the presence of high seismic amplitude anomalies is mainly due to gas saturation has significantly contributed to drilling failure in "Taadoy" Field. To mitigate failure due to seismic amplitude anomalies, it is imperative to analyse the possible presence of tuning effect in high seismic amplitude anomaly in this field. Seismic to Well tie was used to identify reservoir "Res 500". Presence of hydrocarbon anomaly was determined using seismic amplitudes cross-plot and attribute analyses. Rock Physics Template (RPT) helped to substantiate the presence of gas in the thin sand and acoustic impedance inversion revealed minimal impedance contrast between encasing shale and "Res. 500". Wedge model revealed that reservoir "Res. 500" is 10 m thick while the RPT analysis estimated gas saturation of 25%. This implies that the high seismic amplitude anomaly is due to both gas presence and thickness of the reservoir. Amplitudes Variation with Angles (AVA) response indicated high seismic amplitudes at the top and base of the reservoir. The presence of gas causes high seismic amplitude and gradient trends especially at far angles but with minimal effect with increased gas volume. Superposition of seismic amplitudes due to both gas presence and tuning effect produced the high seismic anomaly observed in Res. 500 reservoir.

ARTICLE HISTORY
Received 23 September 2022
Revised 21 December 2024
Accepted 3 January 2025

KEYWORDS
Seismic amplitudes; seismic inversion; tuning effect; gas saturation; seismic anomaly

1. Introduction

The Amplitude Variation with Angle (AVA) or Amplitude Variation with Offset (AVO) analysis is an effective technique for hydrocarbon detection, fluid content prediction and lithology identification (Javaherian et al. 2013; Uko and Emudianughe 2014; Ridwan et al. 2020; Adesanya et al. 2021). The difference between AVA and AVO is that the seismic section in AVA is recorded in angles while the seismic section in AVO is recorded in offset distance. This difference does not have any known effect on seismic interpretation. These techniques are based on the relationship between the coefficient of reflection at an interface and angle of incidence (or offset). These can be varied when there is change in angles or offset distances and magnitude of impedance contrast between the layers (Kamaci and Ciftci 2011; Simm and Bacon 2014; Adeoti et al. 2017). These technique have been successfully applied for quantitative hydrocarbon exploration in many basins including the Niger Delta reservoirs (Osuntola 1996; Hussein et al. 2020). AVO and AVA methods were considered as the second era seismic amplitude interpretation technique following the bright spot era (Allen and Peddy 1994; Hilterman 2001; Allo et al. 2022). This analysis is significant in the development of Direct Hydrocarbon Indicators (DHIs) which are bright spot, dim spot, flat spot, polarity reversal or local phasing and has assisted in the success of exploration projects (Ross and Kinman 1995, Nanda 2016). Despite the successes recorded in the DHI exploration technique, the methods have limitations because other factors that are different from the presence of hydrocarbon can cause DHI reflections (Avseth et al. 2005; Simm and Bacon 2014; Adeoti et al. 2018). Considerable high seismic amplitudes in many sedimentary basins of the world are due to shallow gas accumulation which is expressed as bright spots on seismic data((Allen and Peddy 1994; Kim et al. 2020). Seismic amplitude anomaly gradually decreases with distance from area of accumulation (Ogbamikhumi and Omorogieva 2021). This implies that as gas saturation decreases away from area of accumulation, the precise estimate of its anomaly becomes difficult. Therefore, a more focus analysis of amplitude variations which helps to investigate the cause of high seismic reflections generated from potential reservoir sources is important in establishing gas presence in shallow reservoirs.

Tuning is a phenomenon that refers to the brightening or dampening of seismic amplitude due to constructive or destructive interference of seismic reflections that are overlapping. Tuning effect is the variation in the shape of reflection wavelet during the interference of two seismic events that are related to

CONTACT O.J. Allo allobioje@gmail.com Department of Geosciences, Faculty of Science, University of Lagos, Akoka, Yaba, Lagos, Nigeria

the thinning of a geologic layer (Brown et al. 1986). In other words, when two stratigraphically separated reflectors are close to each other, such that the reflected wavelet from the lower reflector interferes with the reflected wavelet from the overlying reflector, it results in tuning of the seismic amplitudes (Guo 2014; Papageorgiou and Chapman 2020). When times of reflection of seismic traces are recorded along the peaks, troughs or at the zero crossing, tuning effect makes it difficult to measure the accurate arrival times of each reflection events. In many cases, this produces a constructive interference which in turn results to bright spots that are observed as high amplitude anomaly on seismic data (Marzec and Pietsch 2012). The tuning thickness is the thickness of that bed, where tuning effects start to occur especially if the layer thickness is less than half of wavelength (Widess 1973). Moreover, Kallweit and Wood (1982) concluded that as the bed thins to one fourth of the wavelength, the amplitude of the wavelet grows and reaches a maximum, through the constructive interference of the side and main lobes of the wavelet. Tuning makes two reflected signals appear as either one signal or even as no signal. This thickness therefore represents the limit of separability (Roden et al. 2017). The seismic amplitude thus starts to increase and becomes larger than the real reflectivity when the layer thickness is approximately a quarter of wavelength. In this case, the maximum amplitude is reached and there is constructive interference between the top and the base of the layer. Some research findings indicate that except for Class I AVO reflectivity, AVO attributes are significantly altered by tuning effects (Chung and Lawton 1999).

Chopra et al. (2006) demonstrated that when the bed thickness reaches one-eight of the wavelength (λ), that is, $\lambda/8$, the composite wavelet resembles a derivative of the original waveform, and no change in trough-to-peak time will be observed. The seismic amplitude then decreases towards zero as the bed continues to thin. Thin-bed tuning affects both the prestack and poststack seismic amplitudes (Hamlyn 2014). However, depending on the reflectivity sequence, AVO response is significantly altered by tuning effect which could lead to polarity reversal (Chung and Lawton 1999). The high seismic amplitude anomalies caused by the presence of thin bed strata and tuning in seismic data were mitigated by estimating the difference between the peak-to-trough amplitude and the total amplitude. This difference was used to define a transfer function which help to remove the high-amplitude anomalies caused by thin beds (Marzec and Pietsch 2012). AVO analysis of multichannel seismic data was used in the identification of free gas, water-gas contacts and discrimination of bright events among the chaotic signals from tuning (Kim et al. 2020). AVO could be influenced by the contrast in acoustic impedance and Poisson ratio which are associated with the change in fluid saturation. However, the application of this tool needs to consider some influencing factors, including thin bed effects, anisotropy and inelastic attenuation. Tuning effect from the thin bed is the interest of this study.

The general understanding that links observed high amplitudes on seismic data to the presence of hydrocarbon especially gas is becoming more erroneous as geological fields used for hydrocarbon exploration are becoming increasingly complex due to the presence of thin beds. The little emphasis on the ability of the tuning effect to contribute significantly to the observed high seismic amplitude or even in many cases, be responsible for high amplitude has led to drilling of dry holes in "Taadoy" Field with its attendant colossal loss in financial investment. The integrated method adopted in the study has not been deployed before in this field neither has it been reported. In this study, results from AVA analysis, seismic inversion, analysis of tuning effects and wedge modelling were integrated to investigate the impact of high seismic amplitude anomaly from tuning effect due to thin bed and shallow gas saturation amplitude anomaly.

1.1. Basic theory

1.1.1. Amplitude variation with angle/offset

In a two semi-infinite isotropic homogeneous elastic media in contact at a plane interface, incident compressional plane wave impinges on this interface such that reflections at an interface disperses energy from the incident P-wave to reflected and transmitted P-waves (Zoeppritz 1919; Ostrander 1984; Shuey 1985). This also results in reflected S-wave and transmitted S-wave shown in Figure 1 according to Snell's law (Equation 1),

$$\frac{sin\theta_1}{V_{p1}} = \frac{sin\theta_2}{V_{p2}} = \frac{sin\emptyset_1}{V_{s1}} = \frac{sin\emptyset_2}{V_{s2}} = P, \qquad (1)$$

where θ_1 and θ_2 are the angles of incident and transmitted P-wave velocities (V_p) respectively (Figure 1). $\emptyset_1$ and $\emptyset_2$ are the respective angles of reflection and transmitted S-wave velocities (V_s) while P is described as ray parameter (Mavko et al. 2003).

The Zoeppritz equations approximated by Shuey (1985) indicate that the Poisson's ratio is the elastic constant most directly related to the offset-dependent reflection coefficient for incident angles $\leq 30°$. Zoeppritz equation is reduced to Equation 2.

$$R(\theta) = R(0) + Gsin^2\theta + F\left(tan^2\theta - sin^2\theta\right), \qquad (2)$$

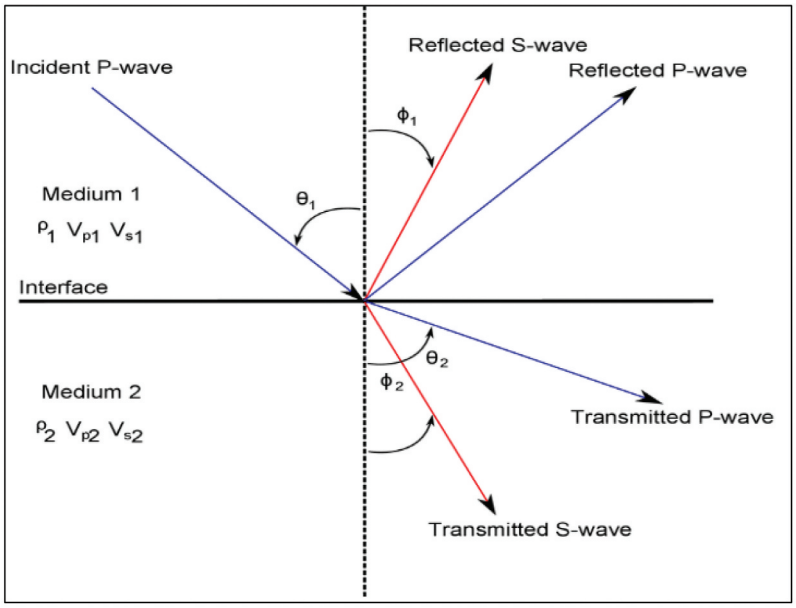

Figure 1. Reflected and transmitted waves at an interface between two elastic media from incident P-wave (Shuey 1985).

where

$$R(0) = 1/2\left((\Delta V_p)/V_p + \Delta\rho/\rho\right); G = 1/2\left((\Delta V_p)/V_p\right) - 2\left(V_s^2\right)/\left(V_p^2\right)(\Delta\rho/\rho + 2(V_s)/V_s); F = 1/2\left((V_p)/V_p\right).$$

Such that, θ is the angle of incidence; V_p is the P-wave velocity in medium; ΔV_p is the P-wave velocity contrast across interface; V_s is the S-wave velocity in medium; ΔV_s is the S-wave velocity contrast across interface; ρ is the density in medium; Δρ is the density contrast across the interface.

When the incidence angle is less than 30 degrees, the third term tends to zero which is obtainable in most seismic surveys. The Shuey's approximation of Zoeppritz (1919) equations becomes Equation 3;

$$R(\theta) = R(0) + Gsin^2\theta. \tag{3}$$

1.1.2. Tuning effect

A thin layer illustrated in Figure 2 showed that t_1 is almost equal to t_2. The first zero offset reflection travels $2t_0$. The second zero offset reflection travels $2(t_0 + \Delta t_0)$. This implies that the change in time due to thickness is Δt_0. The first offset reflection travels $2t_1$. The second offset reflection travels $2(t_2 + \Delta t_2)$. The time difference for the bed thickness is less for greater offset. The tuning thickness is the thickness of the thin bed at which the events from the top and base of the bed become indistinguishable in time. This thickness can be estimated by Equation 4 (Schlumberger 2025),

$$Z = \frac{V}{2.8f}, \tag{4}$$

where Z represents the tuning thickness of a bed (equal to quarter of the wavelength). $V$is the bed's interval velocity while f is the maximum frequency of the target seismic section.

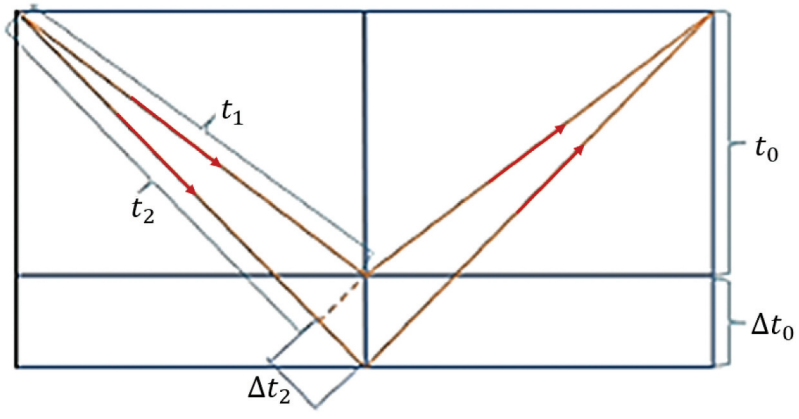

Figure 2. Simplified graphic representative of offset dependency effects (modified from Russell et al. 2006).

2. Geology of the study area

The Niger Delta is a prolific oil and gas province which covers an area of about 75,000 km^2 of southern Nigeria (Kulke 1995). It is situated on the Gulf of Guinea, the West Coast of Central Africa, north of the equator between latitudes 4°N and 6°N, and longitudes 2°E and 9°E (Figure 3). It is bounded in the South by Atlantic Ocean and in the East by the Abakaliki and Calabar Flanks, in the West by the Okitipupa ridge (high) and in the North by Anambra platform (Klett et al. 1997). The basin had its origin closely associated with the rift separating Africa and South America in early Cretaceous times (Evamy et al. 1978; Nwajide 2013). Considering the Pre-Santonian basin evolution of Niger Delta, it seems fairly well established that the oldest Pre-Tertiary sedimentary basin, the Benue-Abakaliki Trough originated as an arm of a triple-junction rift-ridge system that initiated the separation of South America from Africa in the Aptian/Albian. The three arms of the system opened up at different times and at different rates (Weber and Daukoru 1975).

Consequently, to the Campano-Santonian folding, the Benue-Abakaliki Trough was uplifted to form the Abakaliki high, while the Anambra Platform was down warped to form the Anambra Basin (Doust and Omatsola 1990; Cohen and McClay 1995). The Benin flank basement adjoining the Anambra basin was then invaded by the sea for the first time. The formation of the Niger Delta can thus be traced back to the start of Oligocene (early Tertiary), while the present cone-shaped front developed during the Miocene. The thick wedge of clastic sediments beneath the Niger Delta is therefore of early Tertiary to Recent age (Nwajide 2013). The Tertiary sequence of Niger Delta is subdivided into three broad stratigraphic units (Figure 4). They are Benin Formation, Agbada Formation and Akata Formation (Doust and Omatsola 1990).

The Benin Formation is a terrestrial sequence. It is the uppermost and shallowest stratigraphic unit in the Niger Delta. It consists of poorly sorted, medium to fine grained, fresh water bearing sands and conglomerates, with a few shale intercalations which become more abundant towards the base (Adeogba et al. 2005). The thickness of this formation is about 2100 m and, it traps non-commercial quantities of hydrocarbon and has sand percentage of over 80%. The age of this formation is Oligocene (Short and Stäuble 1967). Agbada Formation overlies the Akata Formation and underlies the Benin Formation. It is a paralic sequence consisting of alternation of sands (sandstones) and shales which are the result of differential subsidence, variation in sediment supply and shift of the delta depositional axes which result in local transgression and regression (Weber and Daukoru 1975; Tuttle et al. 1999). This sequence is associated with sedimentary growth faulting and contains the bulk of the hydrocarbon reservoirs (Figure 5(a)). The sand is under compacted and contains autogenic cement materials which allow free movement of hydrocarbon within it (Lambert-Aikhionbare and Ibe 1984). Furthermore, the Akata Formation is abundantly a marine deposit, characterised by uniform shale

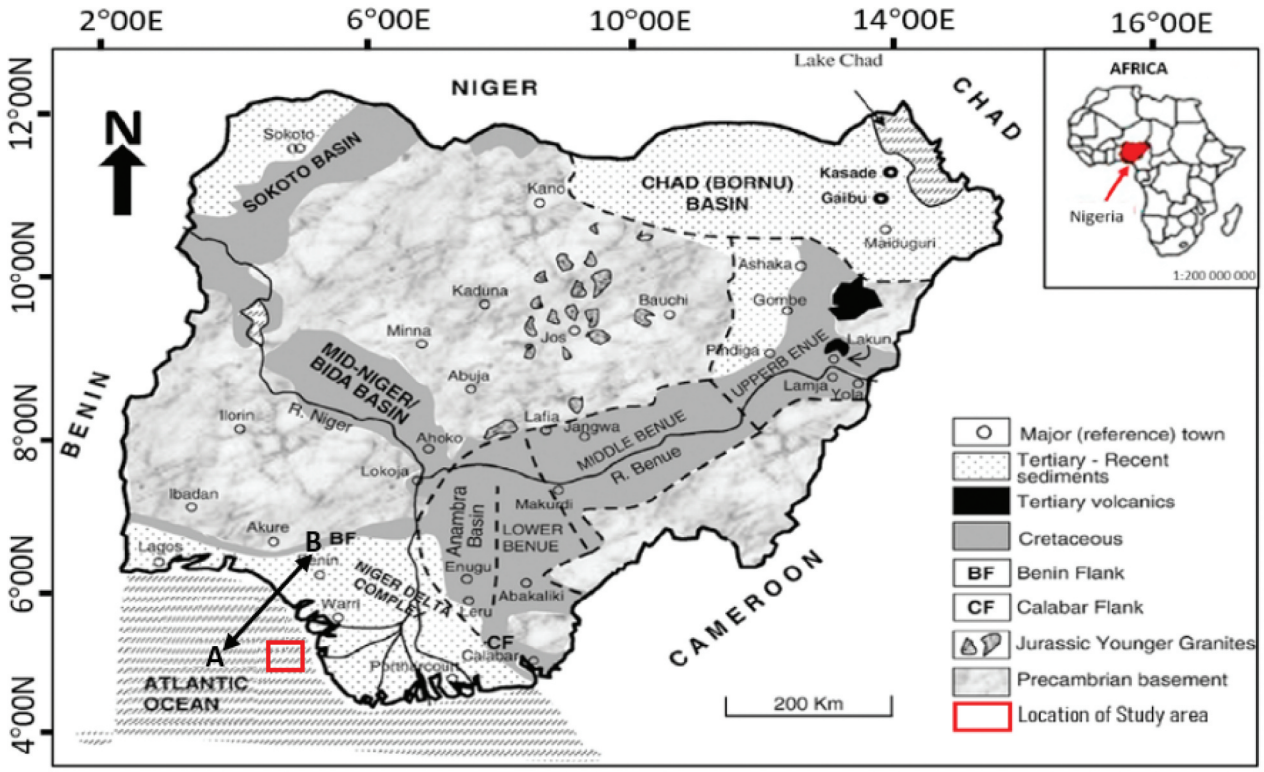

Figure 3. Geological map of Nigeria showing the location of the study area (modified from Obaje et al. 2004).

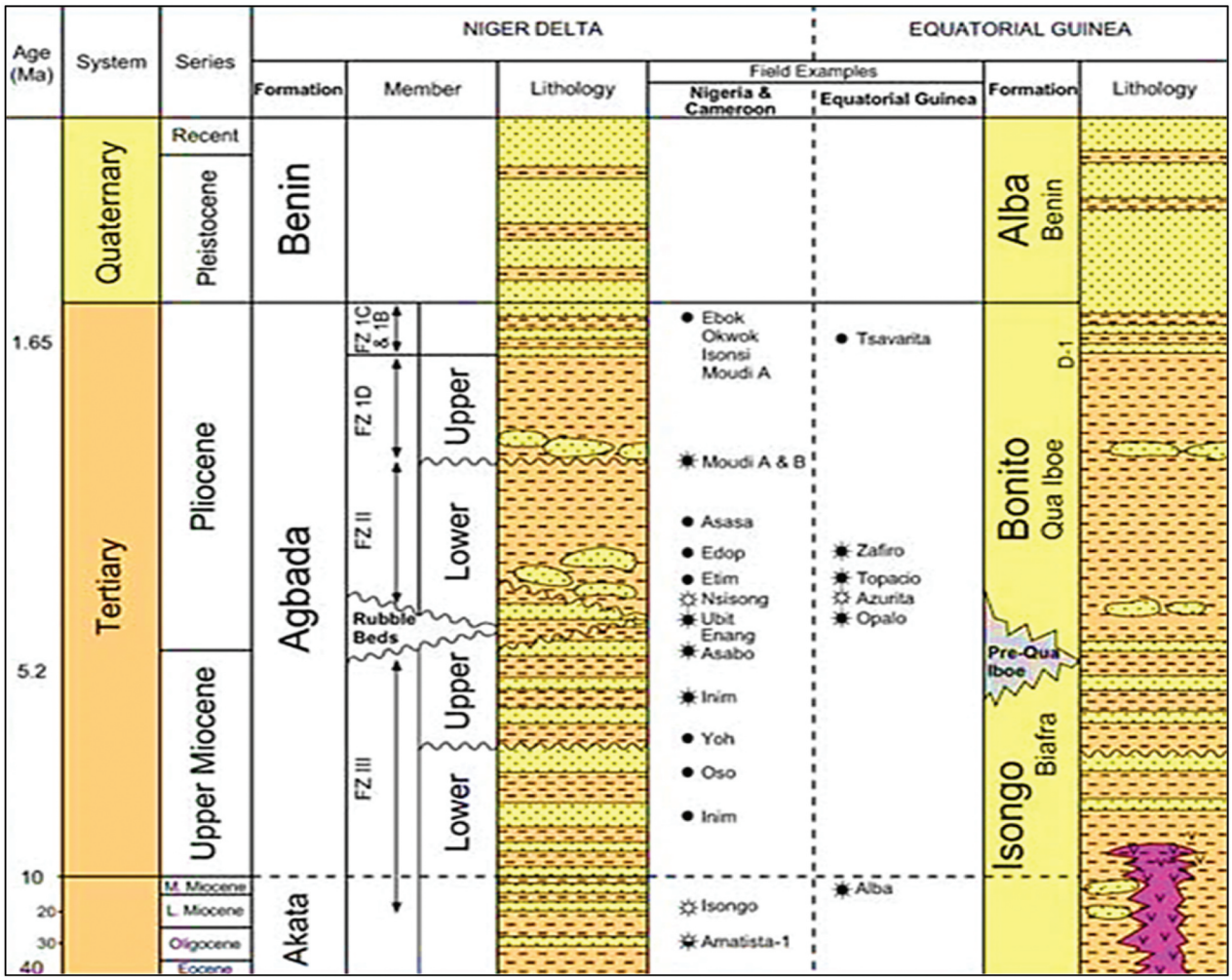

Figure 4. Stratigraphy column of the Niger Delta (Doust and Omatsola 1990).

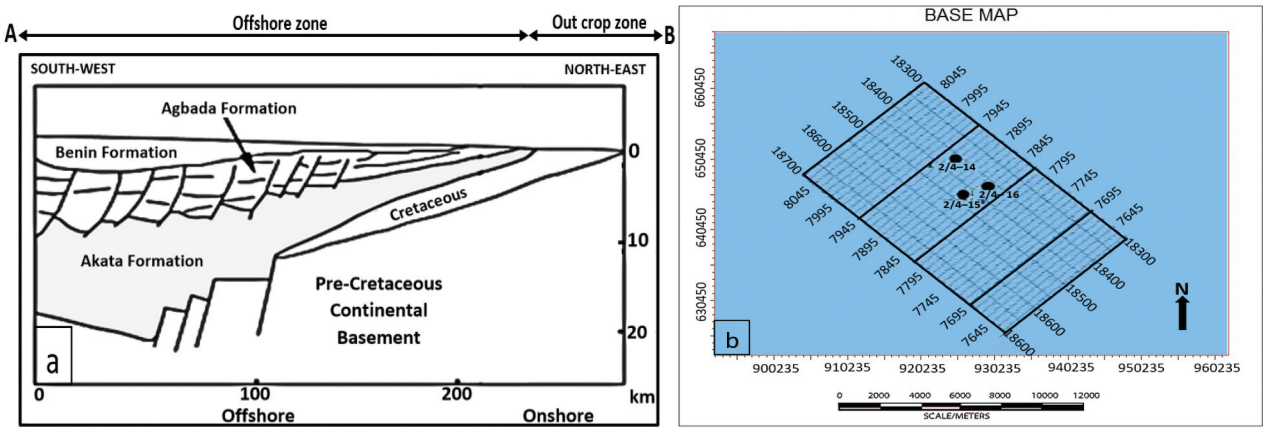

Figure 5. (a) Cross-section across the Niger Delta structural framework. (b) Base map of 'Taadoy' field showing the positions of the three wells.

development with lenses of siltstone and sandstone (Nwajide 2013). It is generally over-pressured. This formation is believed to have been deposited in front of the advancing delta and has a maximum thickness of over 6100 m in the central part of the delta (Kulke 1995). Figure 5(b) is the base map of the Field showing the coverage of seismic survey area and the position of the Well locations.

3. Materials and methods

3.1. Data gathering

A set of post stacked seismic data was provided by the Department of Petroleum Resources (DPR) through Taadoy Geong Limited, Nigeria. The post stacked seismics are data sets in the near (03° to 18°) and far (25° to 45°) angles which are all in the SEGY format. These data were loaded according to the byte locations in the Petrel interpretation software. Three Wells comprising compressional velocity (V_p), spontaneous potential (SP) logs, gamma ray logs, resistivity logs and density logs are provided as shown the base map (Figure 5(b)). Well header information was extracted for correct positioning and loading of the well logs. These parameters were important when loading the data into the geological software, Hampson-Russell and Petrel.

3.2. Data quality control and assurance

Relative seismic amplitude processing was carried out on the angle stacked seismic data to enhance the near and far amplitude ranges respectively. The two stacked data sets were scaled to a common factor to avoid seismic misinterpretations. In the target seismic intervals (horizons) shown in Table 1, the amplitudes show that far and near stacks have similar values of amplitude ratio.

3.3. Data processing

3.3.1. Gas sand detection and thin bed identification

AVA attribute analysis was used to identify hydrocarbon anomalies. This was done by the cross-plot of seismic amplitude of the near angles versus far angles. Seismic amplitude Gradient versus Intercept cross-plot also helped to characterise the AVA class. Furthermore, gas sand zone (top and base), brine saturated and background zone were identified which helped to reveal the corresponding locations in the seismic cross section. The average tuning thickness of the reservoir in this field was estimated through the technique discussed in later sub-section 3.3.5.

3.3.2. Seismic to Well tie

Seismic to Well tie involves matching the seismic horizon to the corresponding Well tops and bases. This helps to correlate seismic events and subsurface log information. The process was done using Well 2/4–16 to optimise the correlation between Well logs and seismic data. The sonic log was de-spiked for appropriate synthetic and original seismic correlation from Well location and minimal time shift adjustment. The correlation window showed improved correlation when a time shift and stretching were applied on the time window between 400 ms to 1000 ms.

Table 1. Numerical calculation of seismic amplitudes scaled factor.

Seismic Interval [ms]	Near Mean RMS	Far Mean RMS	Far/ Near	Amp. Ratio
350–700	1074473967	581128468	1:2	0.54
700–1500	1196441266	614310350	1:2	0.51
1500–2750	1074558788	478514670	1:2	0.45

3.3.3. RMS seismic amplitude attribute analysis

The Root Mean Square (RMS) attribute defines the variation in acoustic impedance over a selected sample interval. The acoustic impedance contrast of lithologies with bed thicknesses above the seismic resolution were identify based on the RMS values. These RMS values are dependent on the acoustic impedance contrast which is the difference in acoustic impedance between two rock layers. This contrast is defined as the ratio of the difference between the product of P-wave velocity and density of the underlaying layer, and the overlaying layer; and the sum of the product of P-wave velocity and density of the underlaying layer, and the overlaying layer. The higher the RMS values, the higher the acoustic impedance contrast between the formations. RMS amplitude analysis was used to distinguish hydrocarbon accumulation observed as high seismic amplitude reflections due to the impedance contrast between lithologies (Allo et al. 2022).

3.3.4. AVA cross-plot and attribute analyses

The class of AVA anomaly observed from the reservoir was determined through the Castagna and Swan (1997) classification. Normalized estimates of the intercept and gradient clusters prevent effects of artefacts and amplitude spikes. Partial angle stacks data were applied to obtain approximations of intercept and AVA gradient as described by Equation 3. The near angle stack data is an approximation of the intercept while the difference of far and near angle stack data was used as an approximation to the AVA gradient (Avseth et al. 2005). The analysis of the change in seismic amplitudes from the near angle stack to the far angle stack was done in a cross-plot of near angle stack versus far angle stack within the time range of 400 ms to 700 ms.

3.3.5. Tuning effect analysis and wedge modeling

A simple wedge model with constant impedance based on the petrophysical or fluid parameter was created to investigate the tuning effect. The P-wave velocity, S-wave velocity and density of the target layer with uniform gas saturation were used as input for the generation of the wedge model synthetic seismograms. In the near and far angles, the ricker wavelets were extracted from the zero phase seismic data. With the Society of Exploration

Geophysicist (SEG) polarity scheme, the start of tuning is the thickness at which the bottom of the wedge begins to interfere with the top of the wedge.

3.3.6. Rock physics template (RPT)

A standard rock property template was used to define the lithology and fluid properties from the reservoir (Res. 500). This helps to provide the spread trend of the rock properties from Well log information. This cross-plot cluster of V_P/V_S versus acoustic impedance from the Well logs was compared with the theoretically developed rock physics template according to ∅degaard and Avseth (2004). The types and volume of fluid, types and trend of lithologies were determined based on the comparative analysis done between the Well log information and theoretically model V_P/V_S versus acoustic impedance relationships.

3.3.7. Seismic acoustic impedance (P-impedance) inversion and reservoir thickness

Near angle stack seismic was inverted using the P-velocity and density to generate P-impedance log needed to produce relative P-impedance inverted seismic volume (Avseth et al. 2005). The purpose of the inversion was to observe the lateral extent of possible presence of shallow gas sand. P-impedance inversion was done using Wells in the time window between 0 to 1000 ms (TWT). Inversion error was reduced through series of iterations. Reservoir thickness distribution was determined through extracted seismic amplitudes from the RMS attributes. The thicknesses of the reservoir at the different Well locations helps to investigate the effect of tuning within the reservoir of interest.

4. Results

4.1. Gas sand detection from angle stacked seismic amplitude

A cross-plot of the near angle stack versus far angle stack helps to check the correlation of the two angle ranges and to test the diagnostic effect of gas presence (Figure 6). The grey rectangle in Figure 6 is the background trend with an approximate directional angle of 45 degree as described in Russell et al. (2006). It implies that the high amplitude red ellipse zone is non-hydrocarbon saturated (base of reservoir) while the blue ellipse represents possible gas sand zone. The corresponding locations of the ellipses are revealed on the lateral seismic time section in Figure 7. Blue ellipse represents the top of the gas sand while the red ellipse represents the base of gas and top of brine saturation. The shallower part of the seismic data (400 ms to 700 ms) shows that far angle amplitude correlates with amplitudes from the near angle based on the resultant discrimination of high, low and background amplitudes in the seismic section shown in Figures 6 and 7.

4.2. Tuning thickness estimation

The zero-phase wavelet extracted from the near stack (Figure 8, top) was used in the synthetic seismic generation where dominant seismic frequency from the target area is approximately 47 hz (Figure 8, bottom), while the estimated velocity from the Well log is 1620 m/s. The thickness of the thin bed which can be observed from the seismic section must not be less than a quarter of the wavelength, that is, $\frac{\lambda}{4}$ (Widess 1973; Simm and Bacon 2014). The average $\frac{\lambda}{4}$wavelength equals;

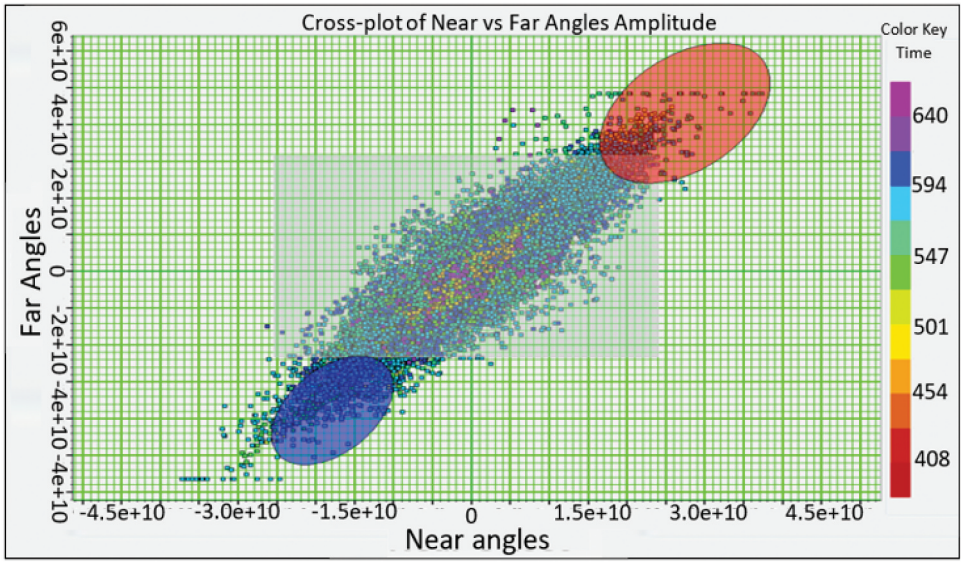

Figure 6. Cross-plot of near versus far seismic amplitude stacks. The color bar shows the two-way travel time. The gray rectangle represents the background trend.

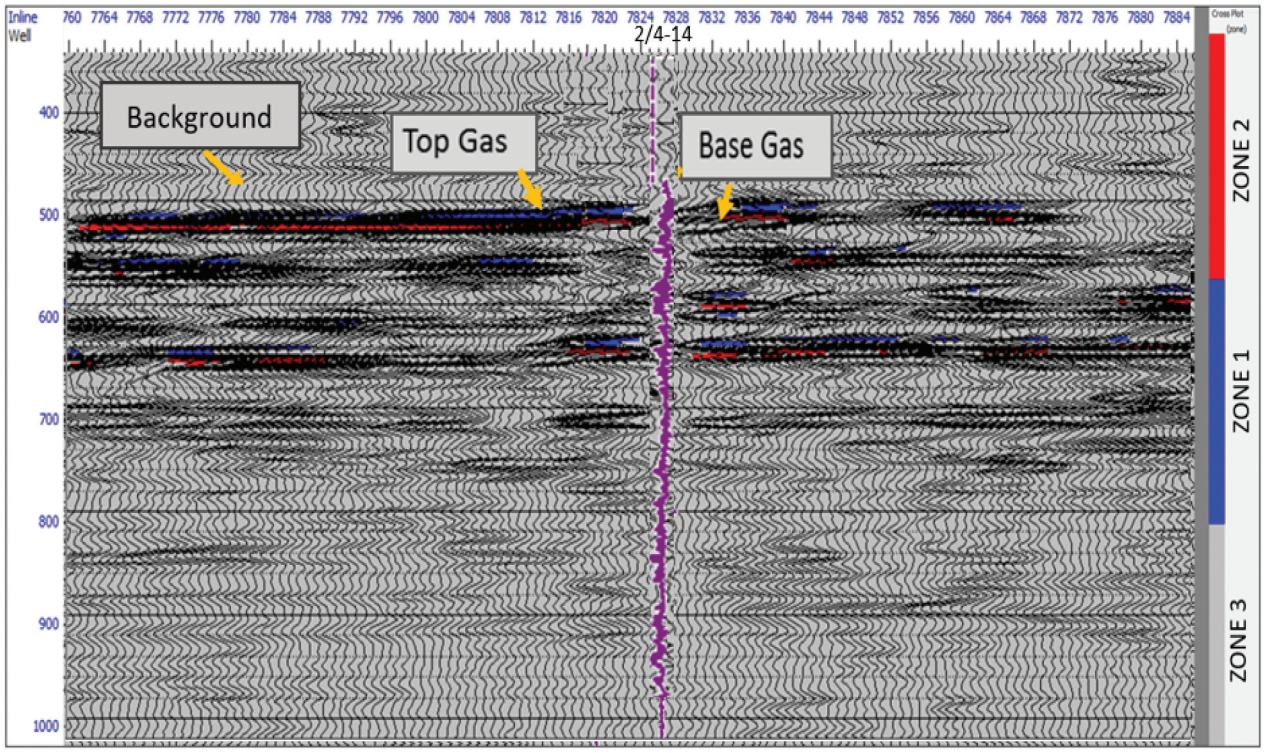

Figure 7. Seismic section showing background, top and base of sand reservoirs. The color bar corresponds to the different highlighted zones (ellipses) in the cross-plot of Figure 6.

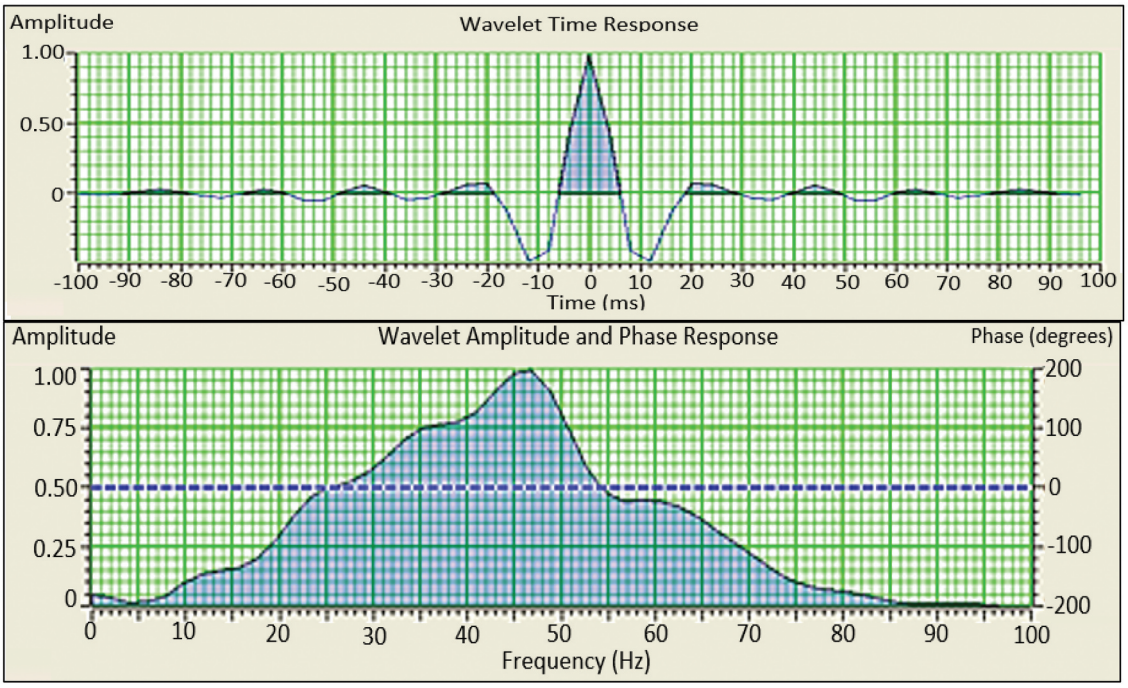

Figure 8. Extracted wavelet (top) and amplitude spectrum (bottom) from the near stack of time range between 400ms to 1000ms.

$$\frac{\lambda}{4} = \frac{[1620/47]}{4} = 8.62m.$$

The mean tuning thickness is therefore;

$$Z = \frac{1620}{2.8 * 47} = 12.31m.$$

4.3. Thin bed identification and seismic to Well tie

Figure 9 shows the corrected Well logs, synthetic seismic and the original seismic (black). The target thin reservoir (Res. 500) is at Two Way Time (TWT) 500 ms and shallow depth of 450 m marked in grey. Blue synthetic traces represent estimates from Well 2/4–14 while the red synthetic traces are estimate from the

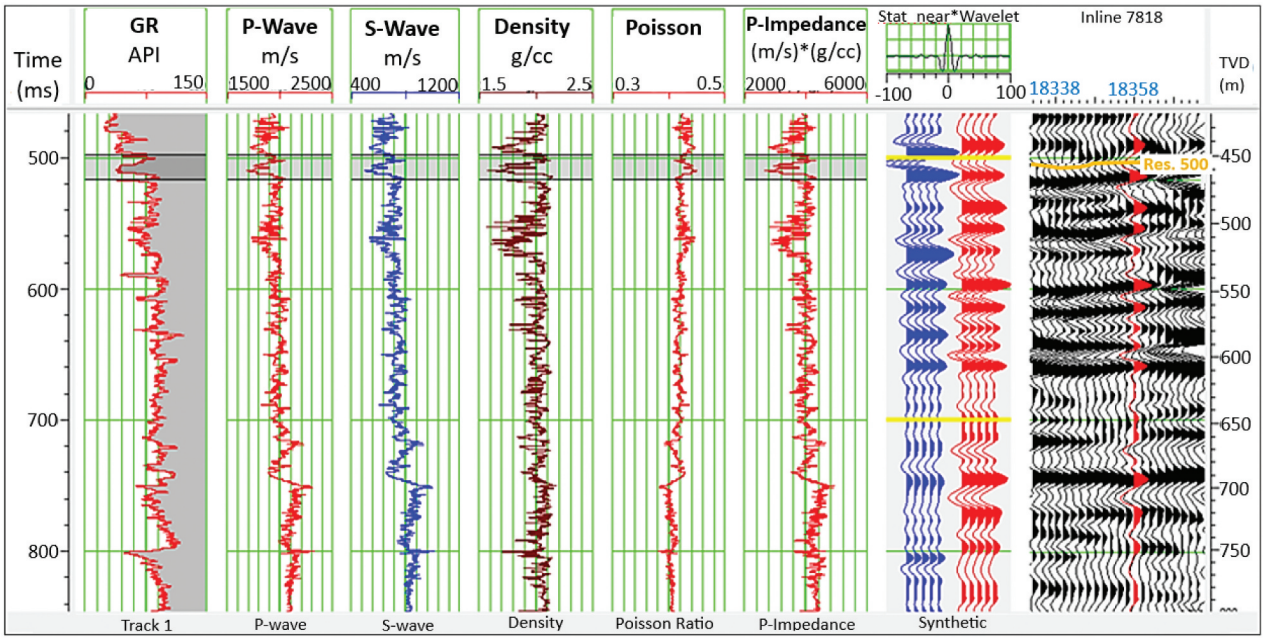

Figure 9. Well to seismic tie at Well 2/4–14. From left to right: gamma ray log, P-wave velocity, S-wave velocity, density log, calculated acoustic impedance and $\frac{V_p}{V_s}$, the synthetic and original traces correlation.

original seismic (Figure 9). The correlation coefficient between the synthetic seismic and the original seismic is 72%, it signifies good correlation.

4.4. AVO class determination of gas sand

Intercept versus Gradient cross-plot of the target horizon (Res. 500) and its corresponding extracted high seismic amplitude cluster are shown in Figures 10(a,b) respectively. Zone of anomaly representing background trend and Class III AVO according to Castagna and Swan (1997) is shown in the Intercept versus Gradient cross-plot (Figure 10(a)). The corresponding location of Class III AVO amplitude anomaly from the seismic horizon is revealed in Figure 10 (b) which represents "bright spot" on the extracted seismic horizon. A Class III AVO anomaly is an indication of the presence of soft sand saturated with hydrocarbon (gas). It implies that the reservoir is characterised by unconsolidated sands especially in the shallow part.

4.5. Tuning effect detection from AVA analysis

High seismic amplitude anomaly from reservoir located at 500 ms (Res. 500) around the Well at depth 450 m is depicted in Figure 11(a). Seismic Inline (7845) and crossline (18562) sections from the far angle stacked 3D seismic reveal the high seismic amplitudes highlighted by white rectangle on the seismic section. Extracted RMS amplitude time slice map from this reservoir is illustrated in Figure 11(b) with two black dashed lines showing the path of the seismic lines at Inline (7845) and crossline (18562). A pinched-out pattern that is referred to as "finger shape" is marked with a white circle. These "finger

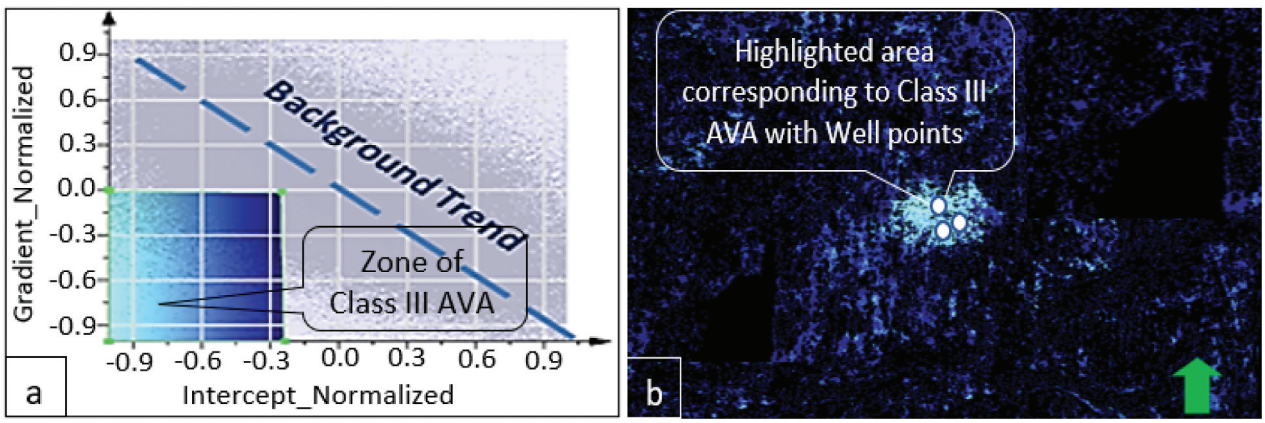

Figure 10. (a) AVA cross-plot showing class III anomaly. (b) The target seismic horizon with corresponding class III high amplitude anomaly.

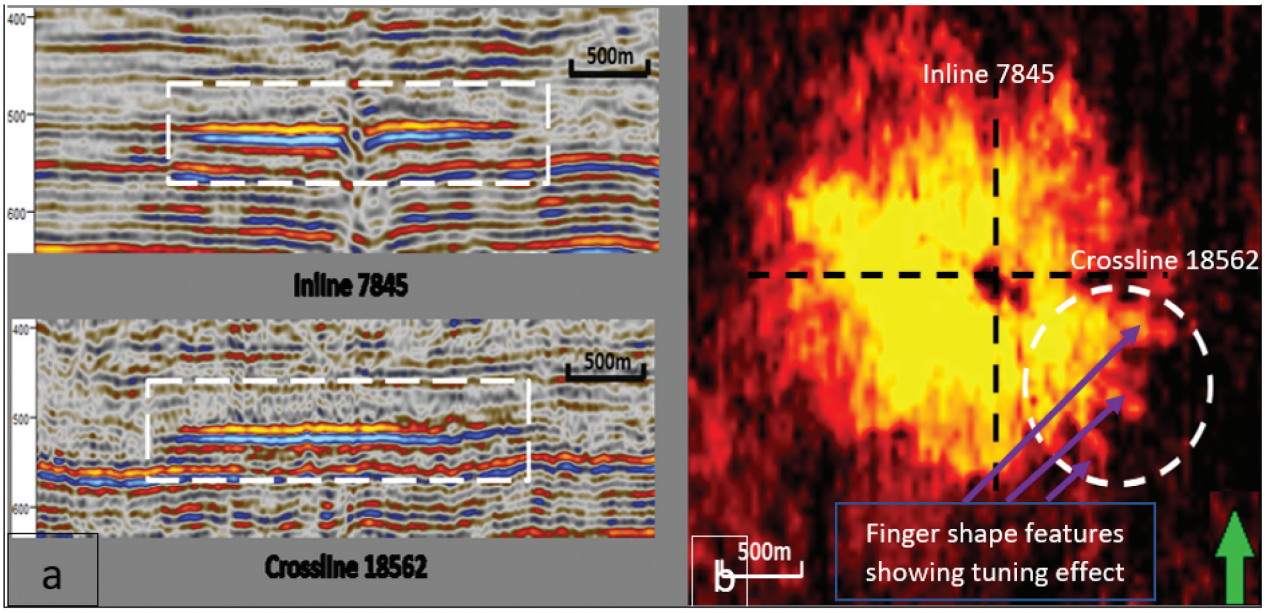

Figure 11. (a) 3D seismic inline and crossline sections around the target reservoir at time 500 ms. (b) RMS seismic amplitude extraction of the target horizon. The marked white circle reveals features referred to as the 'finger' shape.

shaped" features are due to the effect of tuning at the "onset of tuning thickness" around the reservoir. It is an indication that seismic amplitude tuning influences the high amplitude anomaly and also contribute to the observed high seismic amplitude anomaly in this reservoir. The high seismic amplitude "finger-shaped" features is evidence of the probable contribution of the high seismic amplitude anomaly at the "onset of tuning thickness".

Furthermore, the plots of seismic amplitudes against distance from Well 2/4–14 to Well 2/4–16 (860 m apart) as shown in Figures 12(a–d) illustrate one major seismic amplitude peak and more than one minor seismic amplitude peaks. At the distance of 230 m between Well 2/4–14 represented by "A" and Well 2/4–16 represented by "B", the position of the major seismic amplitude peak extracted from the near seismic stack is denoted by the blue dash line (Figure 12(a)). However, slightly higher peak seismic amplitude is detected from the far seismic stack at a distance of 260 m (Figure 12(b)). The slight 30 m shift in distance may be attributed to the difference in the mean of high seismic amplitudes from the far stack compared to the average from the near seismic stack. In both the near and far angle stacks, the seismic amplitude against distance plot reveals similar trend. The various observed peaks from "A" to "B" is an indication of significant constructive interference of seismic amplitudes at different locations. The annular representation of this amplitude interference from seismic section is presented in Figure 12(c). It depicts the amplitude trend from point "A" to "B" in a map view while the corresponding cross-section from point "A" to distance "B" is shown in Figure 12(d) which reveals the approximate location of "onset of tuning thickness" and peak amplitude at tuning thickness. The observed major and minor peaks in these amplitude versus distance profiles fall within the zone of high seismic amplitude anomaly in Figure 11(b). Thus, it supports the contributory effect of seismic amplitude tuning in the observed high amplitude anomaly within the target horizon as explained in Widess (1973), Chung and Lawton (1999).

Moreover, the RMS seismic amplitudes distribution at reservoir located at time 550 ms and corresponding depth of depth 520 m from the near and far angle stacks are shown in Figures 13(a,b) respectively. The far angle stack (Figure 13(b)) is predominantly characterised by high amplitudes compared to the extracted amplitudes from the near angle stack (Figure 13(a)). The influence of tuning effect similar to 'finger shaped' amplitudes is observed from the far angle RMS seismic anomaly are identified by the dashed oval shapes in Figure 13(b). This supports the contribution of tuning effect in the observed high seismic amplitude anomaly. It implies that the area of gas accumulation in the reservoir may not extend to the extremes especially the areas identified by the dashed ovals.

4.6. Tuning effect wedge modeling

The blocked logs from *p*- and S-velocities, density, P-impedance and reflection coefficient (reflectivity) used for the wedge modelling are illustrated in Figure 14. It reveals decrease in the reflection coefficient from the top of the sand (dash rectangle), thereby producing a synthetic trough amplitude trace. Consequently, increase in reflection coefficient

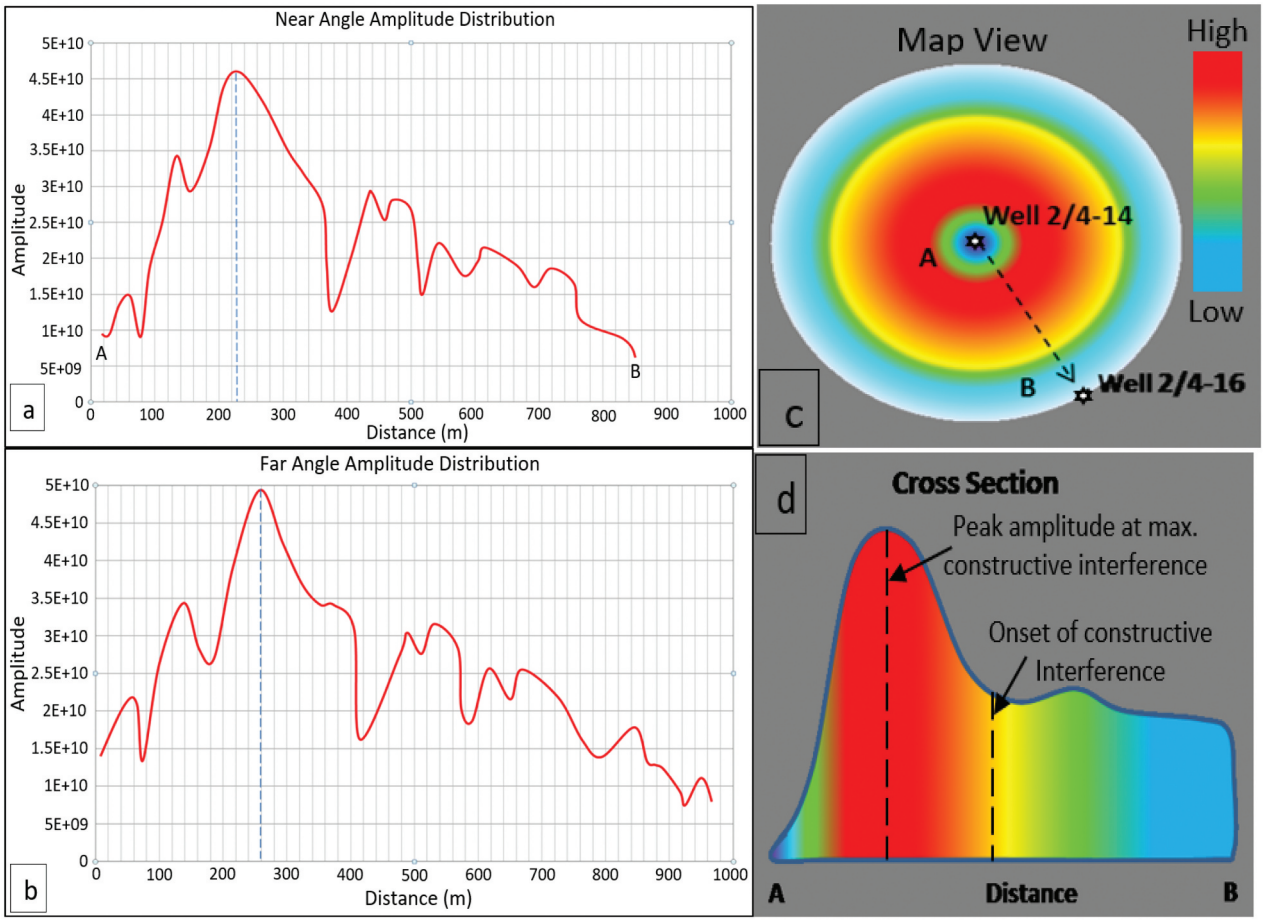

Figure 12. The plot of seismic amplitude against distance from Well 2/4–14 to Well 2/4–16 for (a) near angles, (b) far angles, with the peak amplitude marked by dash line. (c) Annular amplitude representation of far angles seismic amplitude distribution. (d) Cross-section profile of the amplitude distribution showing evidence of tuning effect.

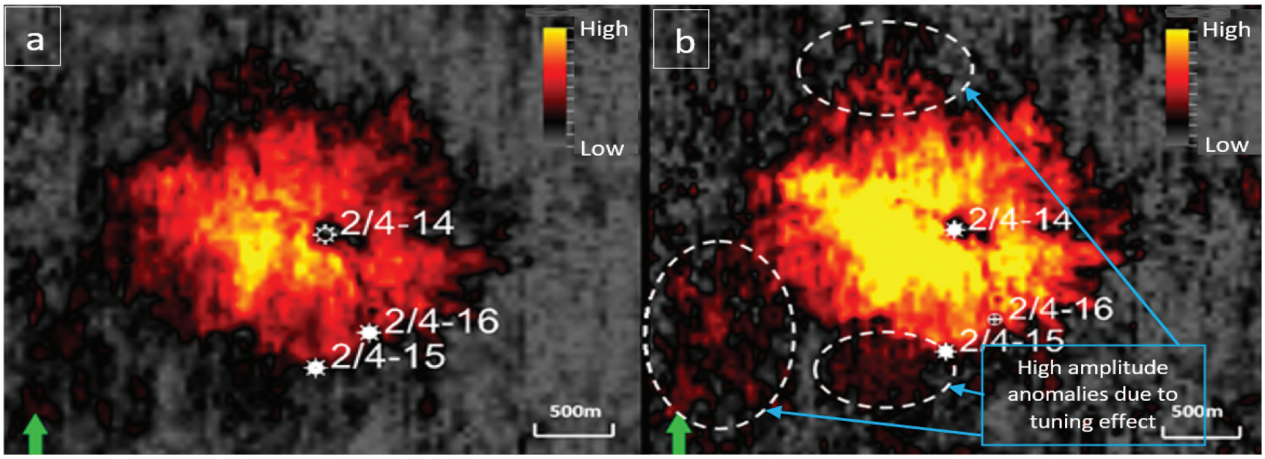

Figure 13. High seismic amplitude anomalies of (a) the near angles and (b) the far angles, showing areas with high RMS seismic amplitude extraction with tuning effect from the target horizon.

results to peak amplitude trace as observed at the base of the sand. The approximate thickness of reservoir sand "Res. 500" from the Well log (Figure 14) is 11 m. This thickness supports seismic amplitude tuning that cause high amplitude anomaly since it approximates the estimated tuning thickness Z which is 12.31 m.

The lithological layers above and below the identified thin bed (Res. 500) have similar acoustic impedance properties such as the density, p- and S-velocities as observed from the Well log data (Figure 14). This produces a schematic representation of a thin layer Wedge model shown in Figure 15(a). As

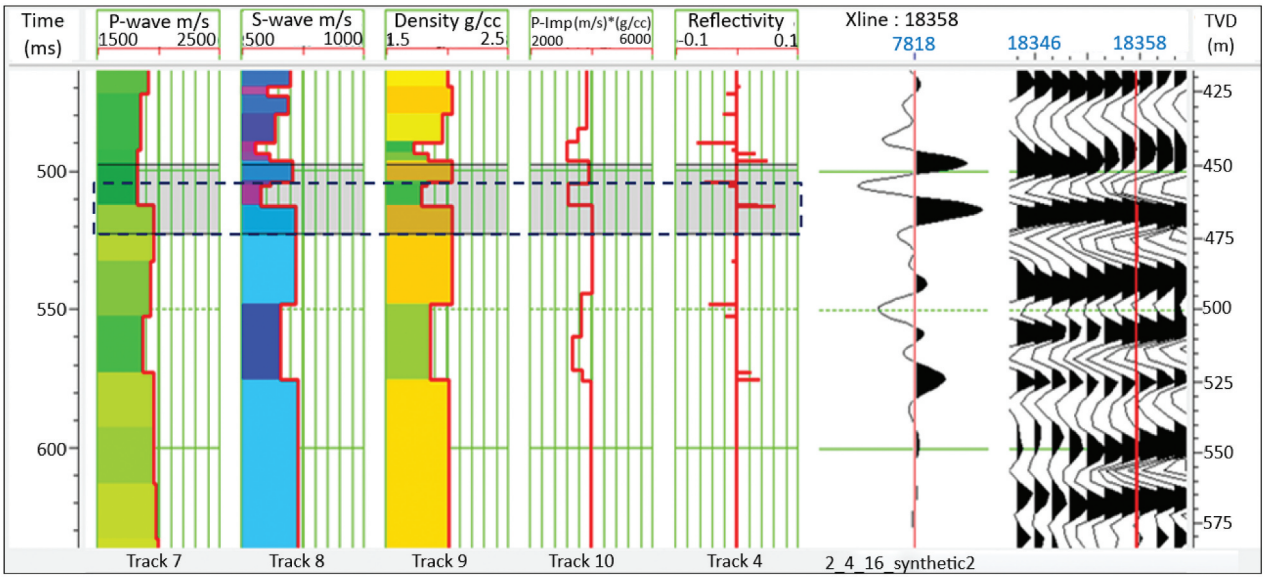

Figure 14. Blocked Well-logs from P-velocity, S-velocity, density, acoustic impedance, computed reflectivity, synthetic trace and far angle seismic stack.

a result of this similarity, the reflection coefficients above and below the thin bed exhibit equivalent magnitudes but opposite amplitude polarities. Figure 15(b) is the generated seismic reflection wedge model with the tuning thickness and "onset of tuning thickness" at approximately 9 m and 16 m respectively. Synthetic seismogram of the wedge model is shown in Figure 15(c) with a wavelet SEG normal polarity convention as indicated by the yellow dashed line. The number at the top of each trace is the wedge thickness of the sand at the location of each trace. Tuning curve of the synthetic seismogram from the top of reservoir is shown in Figure 15(d). It reveals similar values of tuning thickness and the thickness at "onset of tuning" in Figure 15(b). The implication of this wedge model is that reservoir thickness at about 9 m produces maximum seismic anomaly due to tuning effect while the amplitudes are lower at thickness below and above the tuning thickness due to destructive interference.

4.7. Rock physics template (RPT) interpretation of the thin bed reservoir

Reservoir properties such as the density, compressional and shear velocities at Well 2/4–14 are presented in log estimates of V_p and V_s ratio, and P-impedance cross-plot as shown in Figure 16. The overlay of the Well log cross-plot of $\frac{V_p}{V_s}$ versus the P-impedance on the standard cross-plot by Ødegaard and Avseth (2004) helps to identify the shale line and sand, porosity trends of both shale and sandstone reservoirs and also, the presence of hydrocarbon (gas). This cross-plot further revealed that the shallower areas are majorly characterized by brine and shaly sands with minimal difference in acoustic impedance (Figure 16). Difference in the $\frac{V_p}{V_s}$ helps to discriminate shale, gas and brine sands. The red "oval" shape highlights thin sand saturated with gas and the corresponding estimate of $\frac{V_p}{V_s}$ log signature (top right corner) reveals approximately 25% gas volume saturation.

4.8. Wedge model at 25% gas saturation

The characteristic wedge model for 25% uniform gas saturation is shown in Figure 17. Sand top reveals a negative trough seismic amplitude (top reservoir arrow) which implies that higher impedance shale overlays lower impedance gas sand. Yellow dashed lines represent the top and base of the thin sand reservoir respectively, reflection coefficient at the top of the gas sand is therefore negative. Tuning curve from the top of reservoir showed that the tuning thickness is approximately 10 m. The threshold thickness which is the limit of separability is approximately 20 m. As the wedge thinned to less than 10 m, the magnitude of the seismic amplitude decreased rapidly.

4.9. Effect of tuning thickness on AVA response

The wedge model with 25% uniform gas saturation observed in Figure 17 indicates that the magnitude of seismic amplitude rapidly decreases at wedge thickness of less than 10 m. This is due to destructive interference between the amplitudes from the top and base of the reservoir as described by Brown et al. (1986). This effect is illustrated in the generated synthetic AVA response in the plot of amplitude versus angle gather at 2 m, 5 m, 10 m and 25 m layer thicknesses shown in Figure 18. At 2 m thickness of

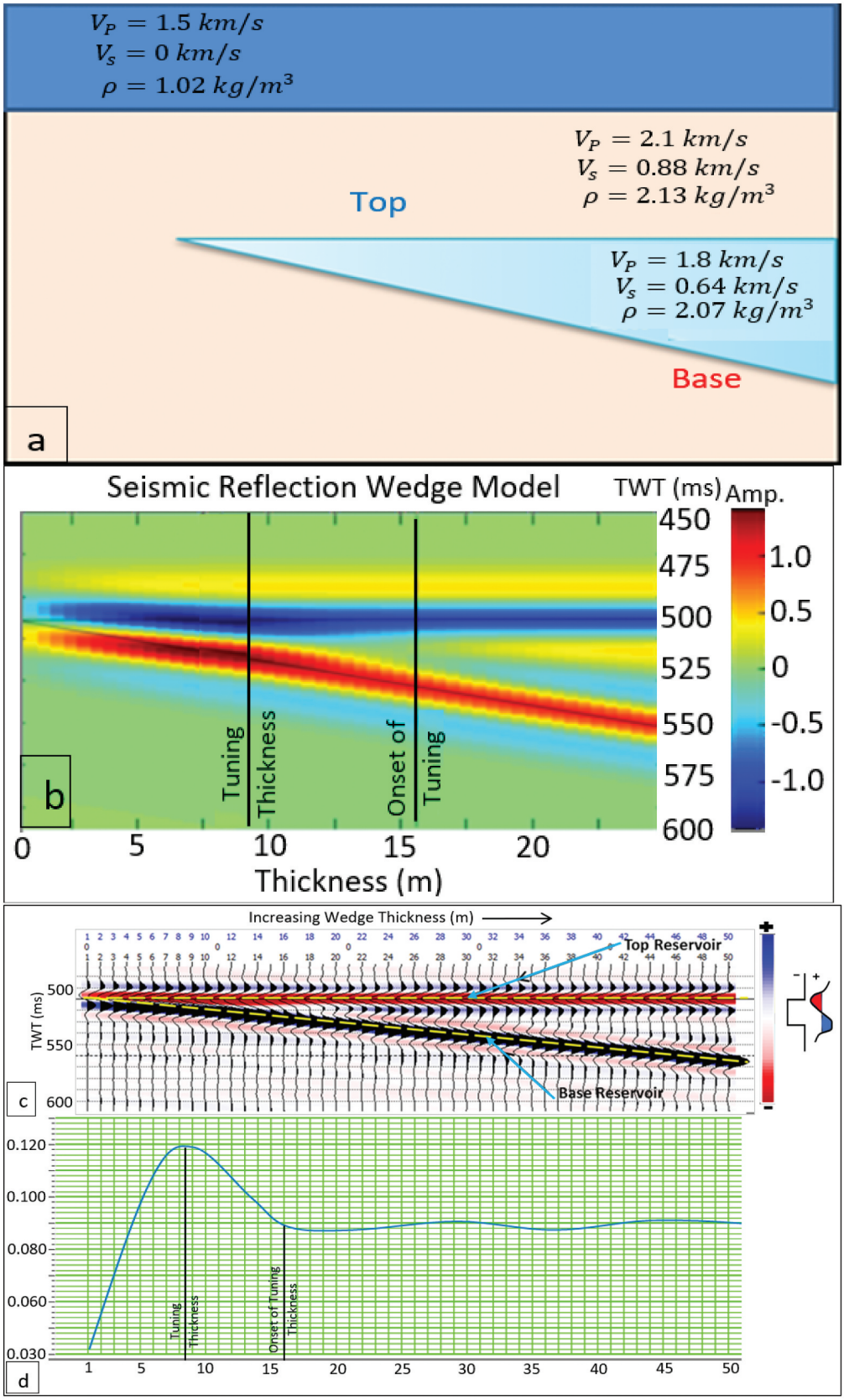

Figure 15. (a) Reservoir properties scheme of the wedge model. (b) Synthetic seismic reflection section of the wedge model showing the tuning thickness and onset of tuning. (c) Synthetic seismogram of the wedge model illustrating the seismic polarities and (d) tuning curve representation of the synthetic wedge model.

the generated synthetic seismic section (upper part), it is difficult to distinguish the trough (red line) from the peak (green line) due to superimposition of the two AVA traces. The AVA response (lower part) from the reservoir top (negative) and the reservoir base (positive) produces a near zero amplitude at zero degree (intercept) with minimal gradient as angle increases in the 2 m thickness model. Similar

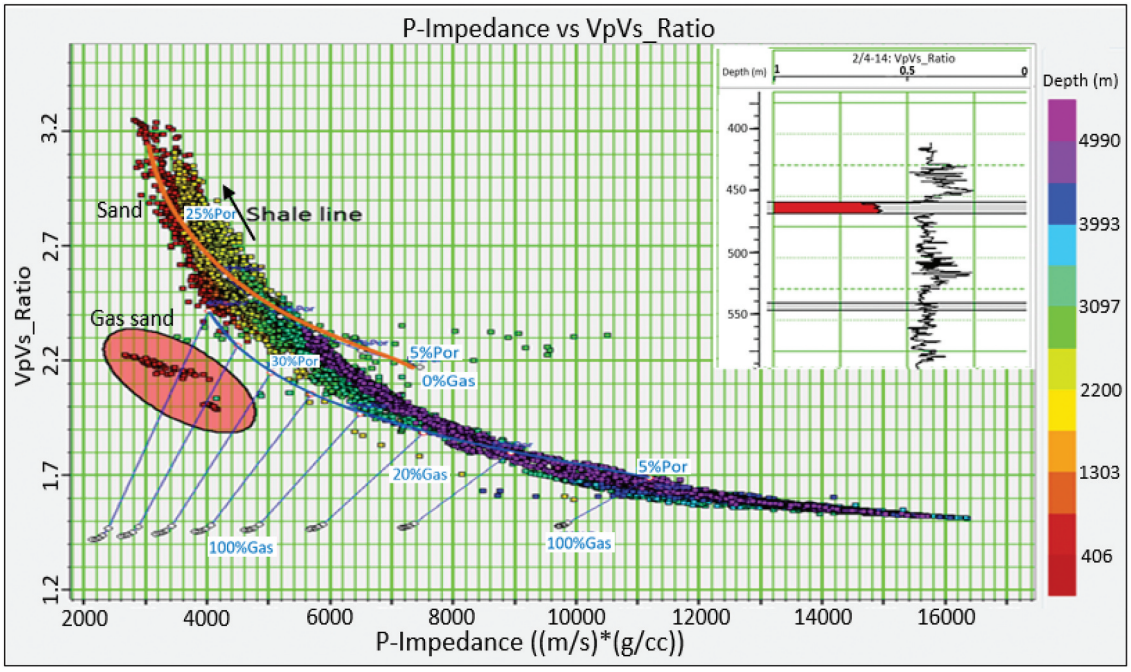

Figure 16. RPT interpretation of the thin sand from Well 2/4–14 using cross-plot of $\frac{V_P}{V_s}$ versus P-impedance. Insert: the corresponding $\frac{V_P}{V_s}$Well section (depth) of the highlight cross-plot area.

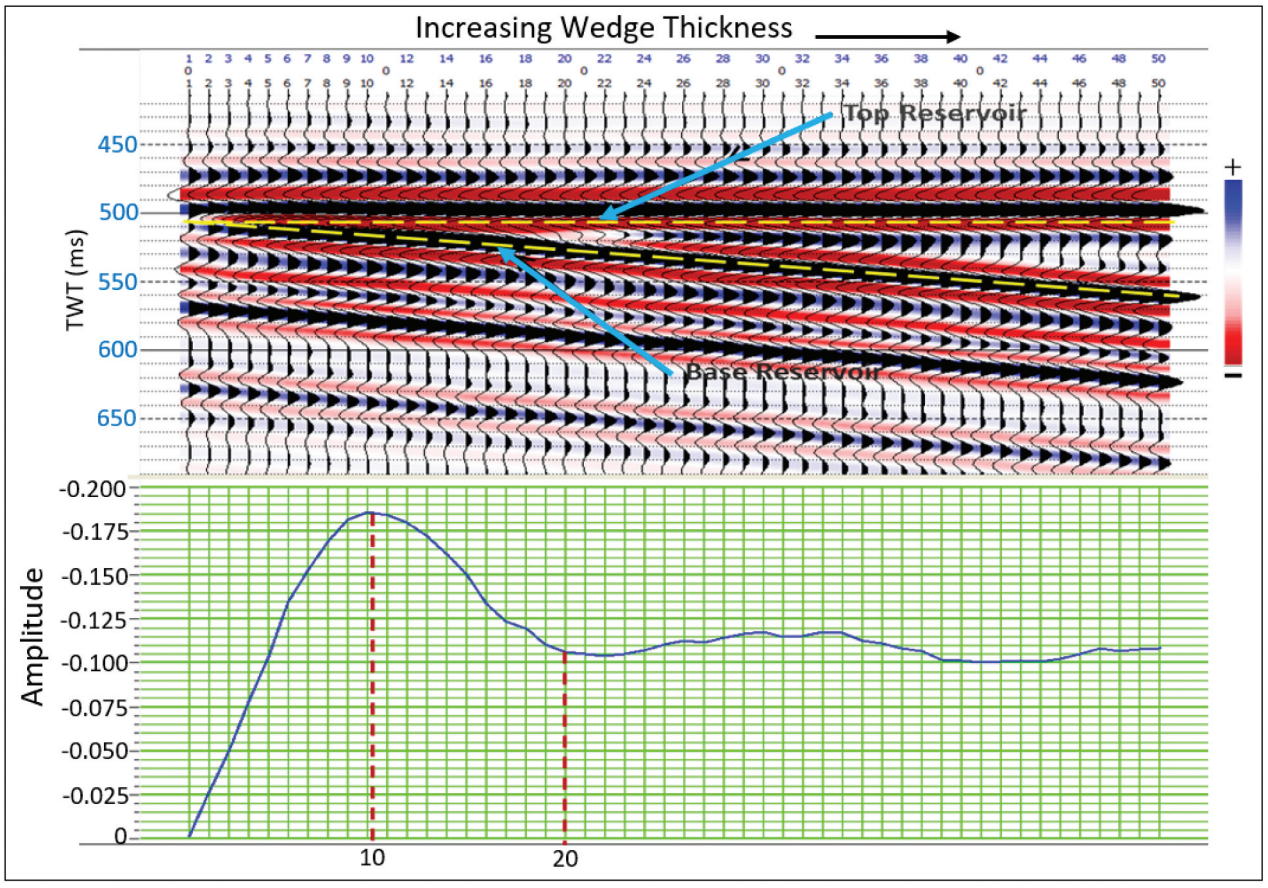

Figure 17. Top: wedge model for 25% uniform gas saturation of the thin reservoir. Bottom: tuning curve of amplitude versus wedge thickness from reservoir top.

response is observed at 5 m layer thickness but with increased amplitude at zero degree. At thickness of 10 m, twice the amplitude value at zero degree of the 5 m thickness is observed and a pronounced high gradient characterises the amplitude versus angle curves. The AVA amplitudes at layer thickness of 25 m (higher than the tuning thickness) reveal amplitude versus angle response that is similar to the

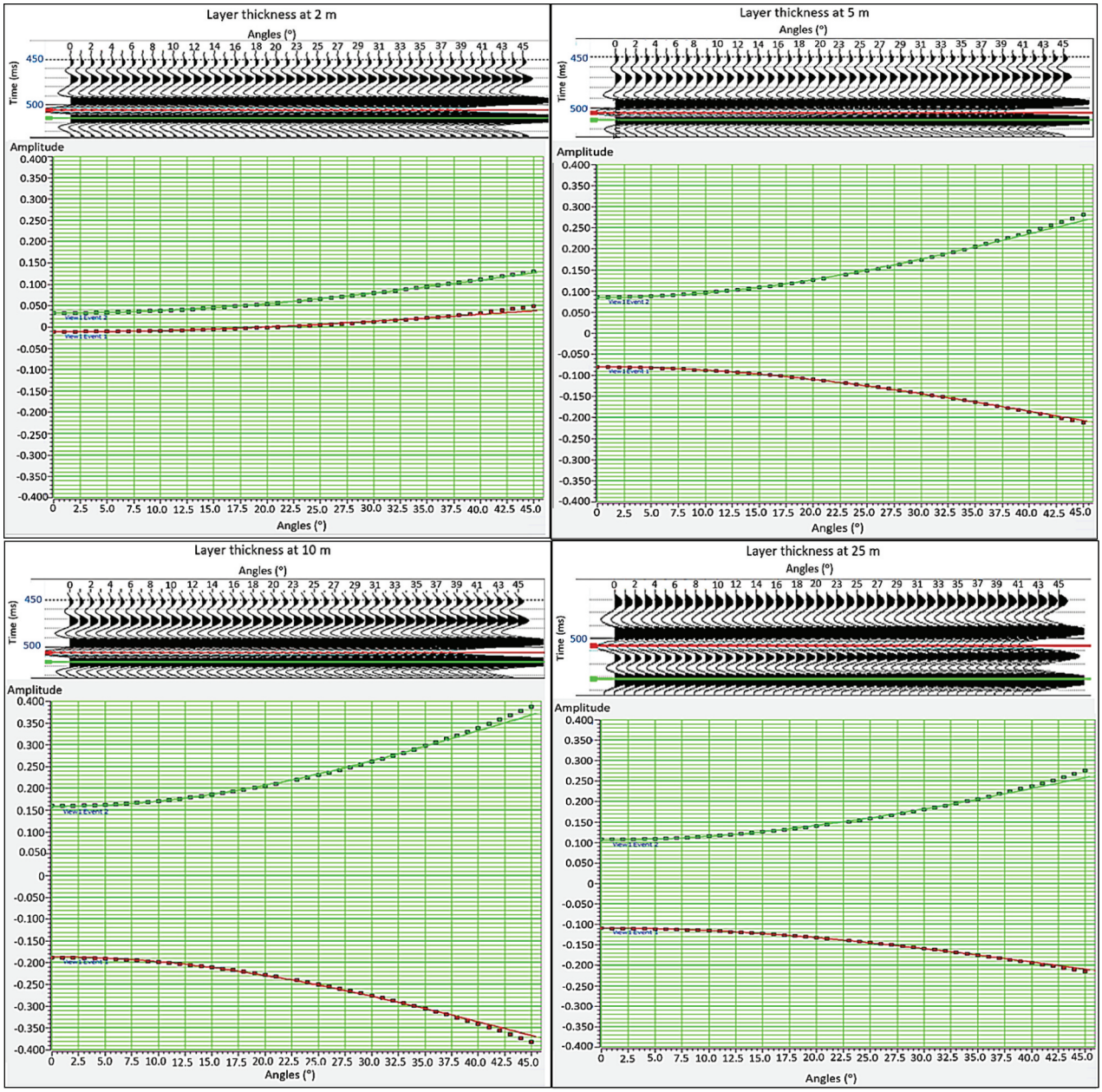

Figure 18. AVA response from angle synthetic gather models at 25% uniform gas saturation. Top left: synthetic AVA and amplitude versus angles plot at 2 m reservoir thickness. Top right: synthetic AVA and amplitude versus angles trend at half the maximum tuning thickness (5 m). Bottom left: synthetic AVA and amplitude versus angles plot at 10 m reservoir thickness. Bottom right: thick sand layer with no tuning effect.

response obtained at 5 m thickness. However, slightly higher seismic amplitudes (trough and peak) are observed which indicate less destructive interference at 25 m layer thickness.

4.10. Fluid effects on AVA and tuning curves

AVA responses for three different cases of 100% water saturation (brine), 25% and 70% gas volumes are depicted in Figure 19. At zero degree, the intercepts are the same, −0.225 for the three cases. The brine saturated reservoir is characterised by relative minimal gradient while the gradients of 25% and 70% uniform gas saturation reveal higher gradient trends. Slight difference is observed in the AVA gradient between the 25% and 70% gas saturations especially at far angles. The large difference in the negative gradient between the brine and gas sands is as a result of change in Poisson ratio of brine to gas filled sands as explained in Allen and Peddy (1994), Simm and Bacon (2014). However, the difference in gas volume only results into minor change in AVA response especially at far angles.

Furthermore, the effect of brine, 25% and 70% gas saturations on seismic amplitudes from the near and far angles are presented in the respective tuning curves shown in Figure 20 (a, b and c). The plot of amplitude versus thickness of the near and far angles reveal similar trends for 100% brine saturation (Figure 20(a)). It implies that no significant

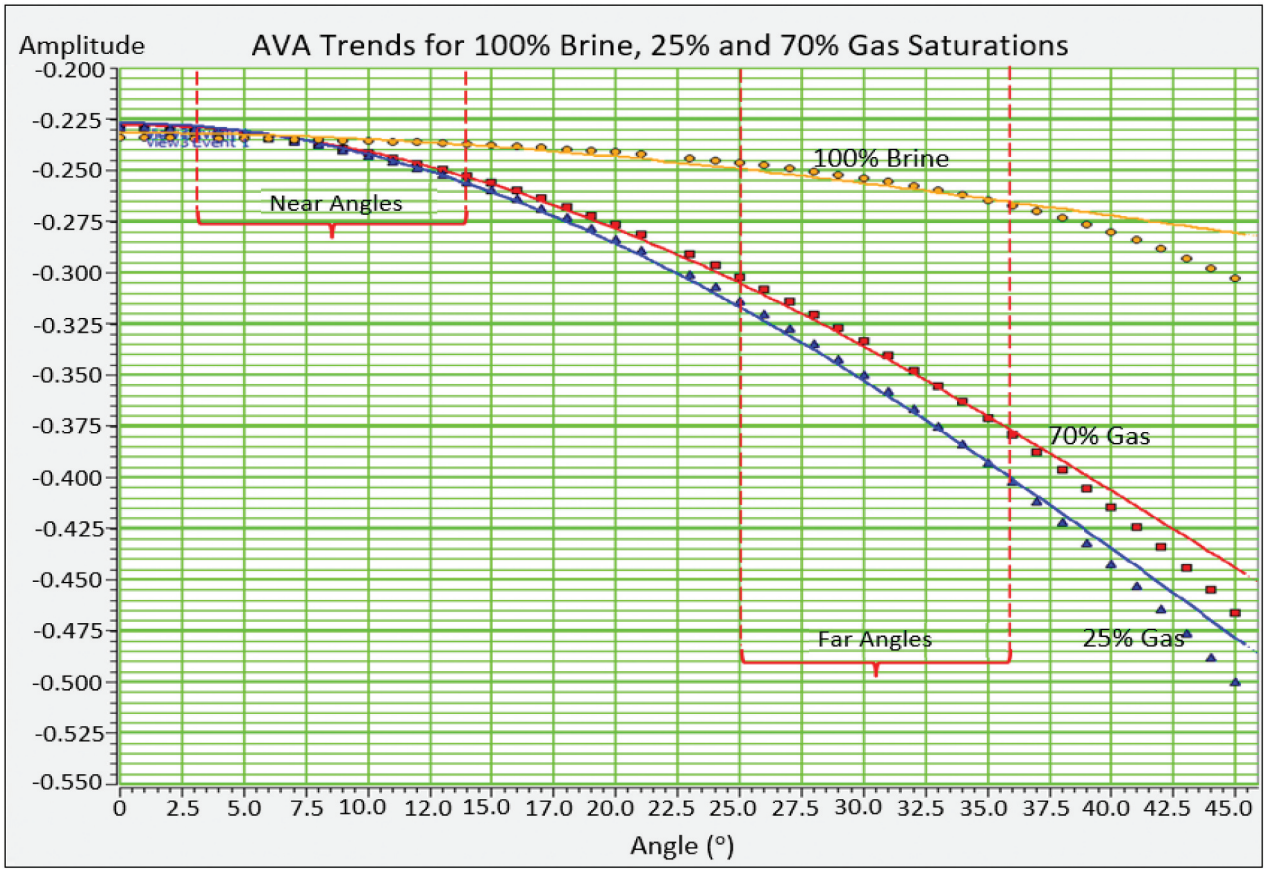

Figure 19. AVA gradient analysis for brine, 25% and 70% gas saturations.

difference in the effect of brine saturation on amplitudes from both the near and far angles. Significant difference is observed between the near and far angles with 25% gas saturation (Figure 20(b)). At about 10 m thickness, the amplitudes of the 25% gas saturation become higher at the far angles. In the case of 70% gas saturation (Figure 20(c)), the near and far angles show similar trends as observed in the 25% gas volume. It confirms that seismic amplitudes increase from near to far angles, which is an indication of presence of gas. Figure 20 also illustrates that increase in gas volume does not have significant effect on the seismic amplitude response especially at the near angles as observed in Figure 19.

Moreso, the amplitude versus thickness plot of the tuning curves at the near and far angles of the brine (100% water), 25% and 70% gas saturations on the same plane is shown in Figure 21. The far and near angles 100% water saturations, and near angles 25% and 70% gas saturation curves produce tuning curves that are closely related. While at far angles, similar trends of higher amplitude tuning curves for 25% and 70% gas saturation are observed. Figure 21 helps to clearly distinguish high seismic amplitude anomaly produced by tuning effects from high seismic amplitude anomaly due to gas saturation. The seismic amplitude anomaly as a result of tuning effect is "high" at 10 m tuning thickness while the anomaly from gas saturation is "higher" at same thickness.

4.11. Inverted seismic amplitude P-impedance contrast

The inverted seismic acoustic impedance (P-impedance) volume derived from the integration of seismic data and acoustic impedance log reveals the impedance contrast of the thin bed (Figure 22). The black ellipse shape around this thin bed shows the area that has been enlarged for better visibility of the target bed. The thin bed gas sand at 500 ms is characterised by relatively low acoustic impedance. P-impedance reduces from the surrounding layer to the gas sand. Figure 23 is the time slice of the thin bed at 500 ms which reveals that the impedance contrast between the gas sand and the surrounding shale is mild. The black square shape is an enlarge area around the Wells, it provides better resolution of the impedance distribution. This reveals that impedance contrast largely ranges between 3400 m/s*g/cc and 3680 m/s*g/cc. It is evidence that significantly high seismic amplitude anomaly from the thin bed is not only due to gas saturation but also as a result of tuning effect in the target area. It implies that other factors such as tuning effect have increased the

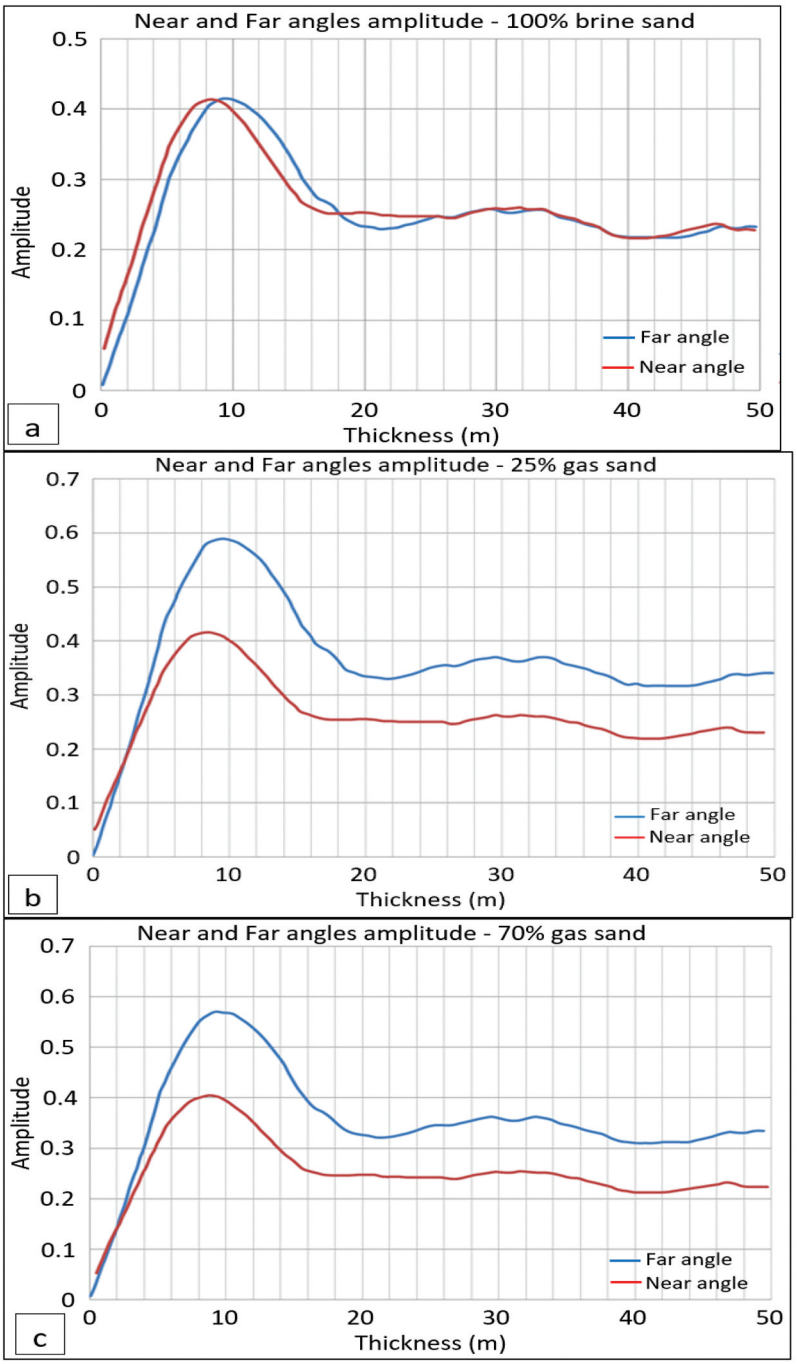

Figure 20. Near angles and far angles amplitude versus thickness plots of brine, 25% and 70 gas saturated reservoirs.

magnitude of seismic amplitude anomaly observed from the thin sand.

4.12. Reservoir thickness distribution

The reservoir thickness distribution of the thin gas sand around the Well locations is illustrated in Figure 24. Near and far angle stacks reveal similar thickness anomalies distribution. Near angles stack thickness map indicates low thickness range is between 8 m and 14 m (Figure 24(a)) while in the far angles stack, a high-resolution thickness anomaly with similar low thickness range is observed (Figure 24(b)). The thickness resolution from the far angles stack is preferable because of the enhanced seismic amplitude anomaly. Reservoir thickness is approximately 10 m around the Well 2/4–14 location. This finding supports the result obtained from the wedge model with 25% uniform gas saturation in Figure 17. The thickness of the reservoir at Wells 2/4–15 and 2/4–16 are approximately 15 m and 18 m respectively.

5. Discussion

The change in seismic amplitudes from the near to the far angle stacks helps to detect the presence of gas sand as revealed by the plot of near versus far seismic amplitudes (Figure 6). It revealed the tops and bases

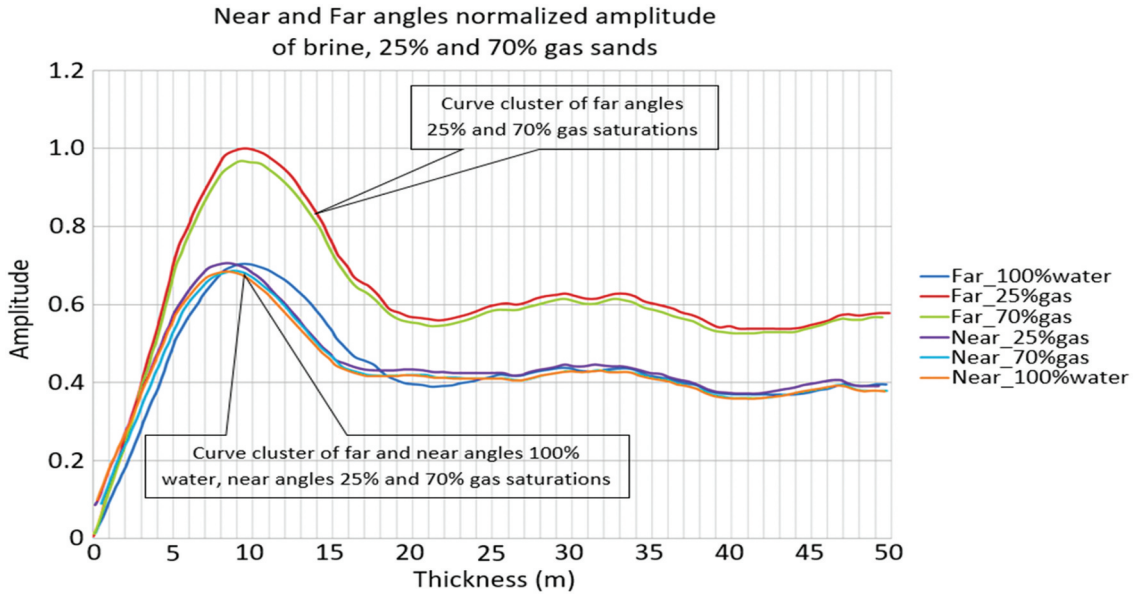

Figure 21. Seismic amplitude and thickness of near and far angle plots of brine, 25% and 70% gas saturations.

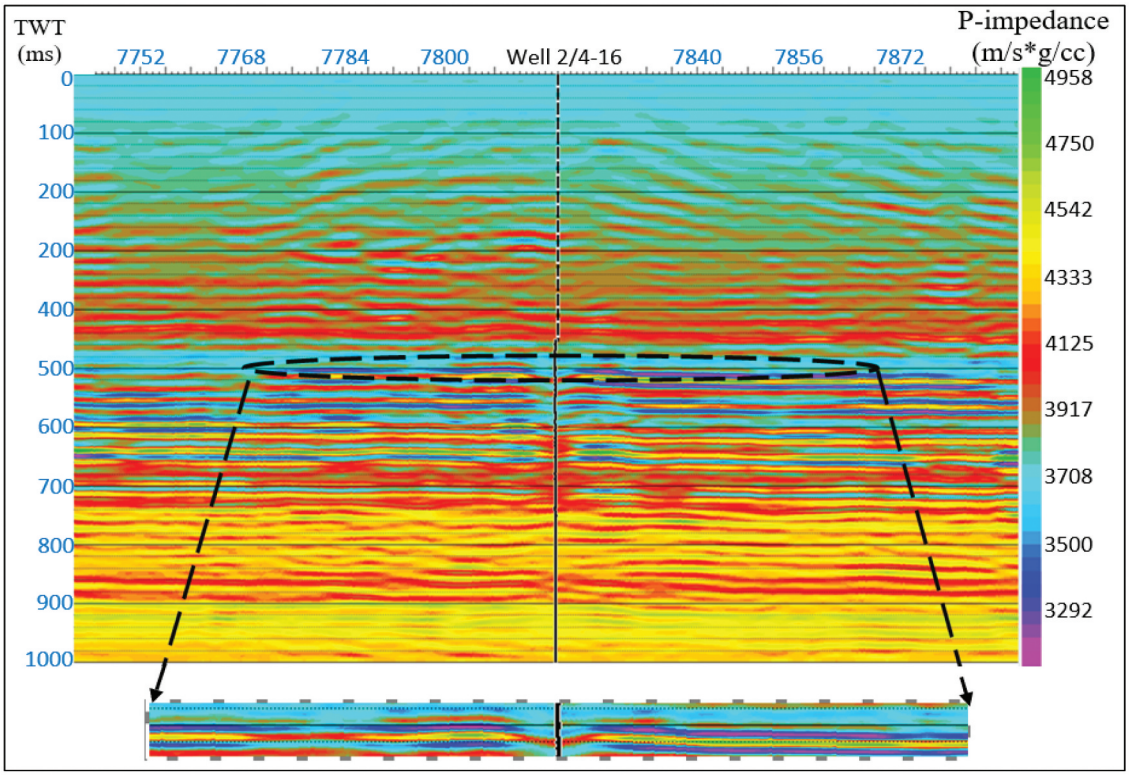

Figure 22. P-impedance seismic inversion highlighting the target horizon, color coded with the impedance values.

of a thin bed within the shallow subsurface layer of the Field (Figure 7). This study focused on a thin sand, "Res. 500" which is located at time 500 ms. The wedge model reveals the thickness of the bed while the AVA analysis helps to detect gas presence, AVA class and tuning effect at different thicknesses of the thin beds. Also, the effect of fluid types and volumes are analysed using AVA responses and tuning curves.

A quarter of the predominant seismic wavelength is estimated as 8.62 m, this means that the seismic signal within the Field can detect the top and base of lithological layers that is not less than 8.62 m thick. Crossplot of intercept versus gradient showed that Res. 500 thin sand is a typical Class III AVA sand (Figure 10). This supports the presence of gas in a soft shallow sand surrounded by hard shale. The acoustic impedance reduces from shale to thin sand resulting to decrease in impedance and high negative seismic amplitudes that increase with angles as discussed in Castagna and Swan (1997). The observed high seismic amplitude is not due to the presence of gas only but

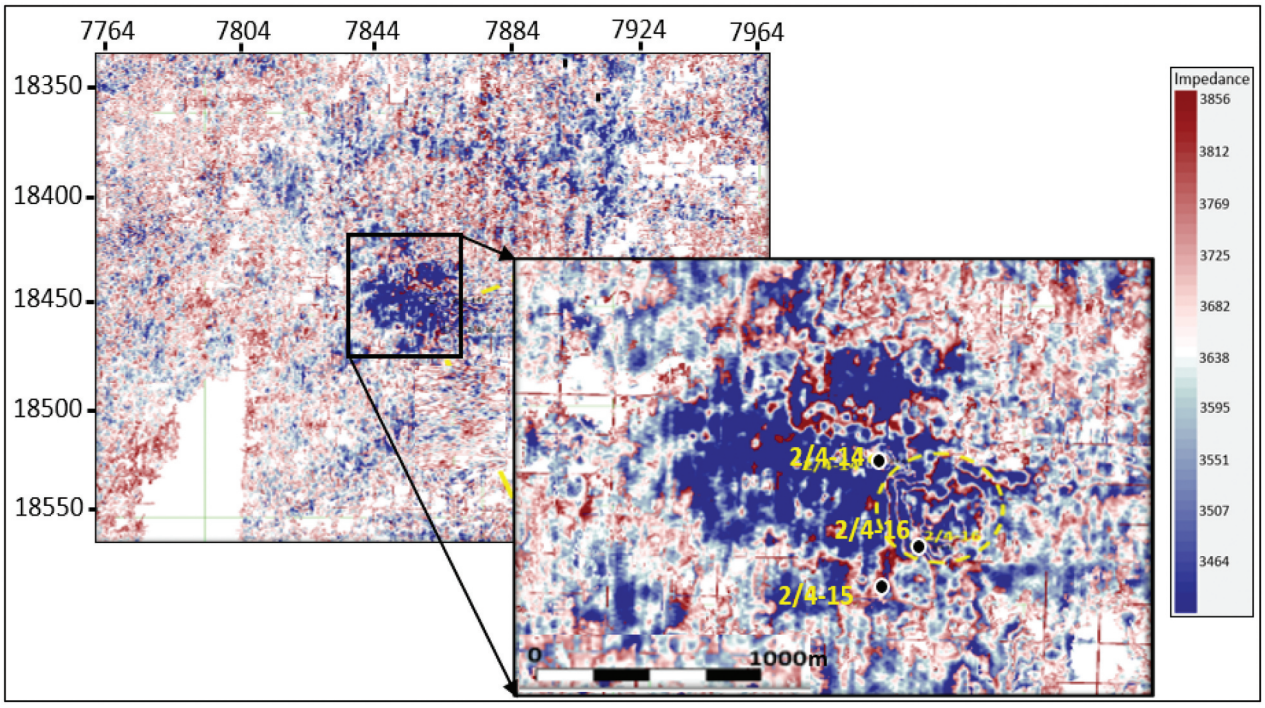

Figure 23. P-impedance inversion time slice of the thin bed at 500 ms showing mild difference in the acoustic impedance distribution around the wells.

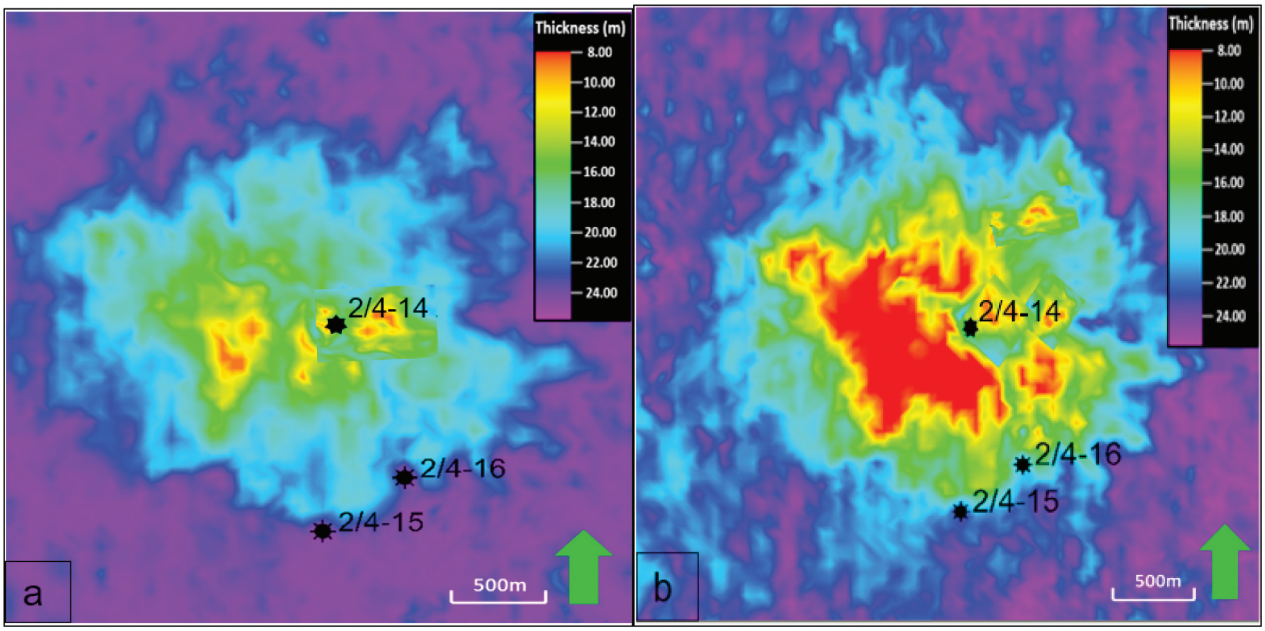

Figure 24. Reservoir thickness distribution of thin gas sand reservoir showing well locations. (a) Reservoir thickness distribution for near angle stack (b) reservoir thickness distribution for far angle stack.

also high amplitudes caused by tuning effect. "Finger shaped" features identified in Figure 11 and multiple peaks of seismic amplitudes (Figures 12 and 13) are evidences of the presence of tuning effect that aided the high amplitude anomaly in "Res 500". The presence of minor peak anomalies between Wells 2/4–14 and 2/4–16 shows that constructive inference from "Finger shaped" and seismic amplitudes from the "onset of tuning" support the influence of tuning effect on the observed high amplitude anomaly. The wedge model (Figure 15) revealed that at about 9 m thickness, the thin bed produced the maximum seismic amplitude anomaly. Below and above this thickness, the seismic amplitude anomaly gradually reduces. This suggests that the thin beds with this approximate thickness range would have been significantly influenced by tuning effect.

Rock physics template of Ødegaard and Avseth (2004) through the cross-plot of $\frac{V_p}{V_s}$ versus P-impedance reveals approximate 25% gas saturation. Figure 16 shows that the gas sand cluster deviates from other shallow sands as defined by the depth color codes. The depth of the sand is about 460 m as depicted by the $\frac{V_p}{V_s}$ log section. $\frac{V_p}{V_s}$ provides significant discrimination between gas sand and other shallow sands. At 25% gas saturation, the tuning thickness and "onset of tuning thickness" slightly shifts to 10 m and 20 m respectively. The marginal change in thicknesses is as a result of increase in seismic amplitudes due to the presence of gas in the thin sand. The average high negative seismic amplitudes due to gas presence resulted into slight shift in the mean thickness and "onset of thickness" estimates as shown in Figure 17. Therefore, the values of the thicknesses obtained from the 25% gas saturated wedge model provide a reliable estimate of the tuning thickness of the thin sand.

Tuning effect from thin sand is further investigated from the AVA responses of layer thicknesses at 2 m, 5 m, 10 m and 25 m. Similar amplitude versus angle trends is observed from the top and base of the 2 m thin sand. In this case, the top of the sand produced a positive (peak) while the base revealed polarity crossing from negative to positive (Figure 18). This is a consequence of seismic amplitude superposition where the negative reservoir top interferes destructively with the positive reservoir base which makes a 2 m gas sand appears as a positive peak amplitude in the synthetic seismic session. The amplitudes and gradients of the 5 m thin sand reveal gradual increase with angles, while in the 10 m sand layer, the increase in amplitude and gradient is more significant. This illustrates the existence of constructive interference between the negative trough from the reservoir top and positive peak from the reservoir base which increases with increasing angles. At this thickness, the reservoir exhibits high seismic amplitude anomaly which enhances the observed bright spot from the gas sand. However, the 25 m layer thickness revealed reduction in the amplitudes and gradients from the top and base of the sand layer. It implies that no constructive interference that could lead to enhance seismic amplitudes occurred at this thickness.

Gas presence in the thin sand is substantiated by the different AVA curves in the amplitude versus angle plot (Figure 19). Variation in gas volume has minimal change in the AVA response while the response between brine and gas saturations revealed significant discrimination. The presence of gas results to high seismic amplitudes especially at far angles. Similar scenario occurred in the tuning curve plot of amplitude versus thickness where seismic amplitudes are higher at far angles especially at 10 m thickness. Figure 21 illustrates that gas sand at far angles is characterised by higher seismic amplitude anomaly compared to the brine and near angles responses from gas sand at 10 m thickness, although, both gas sand and tuning effect resulted to high seismic amplitude anomalies. However, the acoustic impedance contrast between the reservoir (Res. 500) and the encasing layer is minimal as revealed in Figure 23. This supports the influence of tuning effect in the high seismic amplitude anomaly observed from the thin gas reservoir. Area distribution of reservoir thickness is shown in Figure 24 where the thickness range between 8 m and 10 m produced the highest range of high seismic amplitude anomaly. The magnitude of seismic amplitude reduces with increasing reservoir thickness as shown in both Figures 11a and 24.

6. Conclusion

The seismic amplitude anomaly from thin gas sand reservoir (Res. 500) was investigated to ascertain the presence of tuning effect on the observed high seismic amplitude anomaly. This reservoir is characterised by a Class III AVA which makes the gas sand to produce a negative high seismic amplitude anomaly. In this study, the observed anomaly was found not to be due to the presence of gas only but also due to the influence of seismic amplitude tuning from average reservoir thickness of 10 m. The wedge models and tuning curves revealed that at about 10 m layer thickness, gas sand seismic amplitudes interfere constructively resulting into high seismic amplitude anomaly. AVA response at 10 m thickness produced significant high amplitude and gradient which supports constructive interference at this thickness. Although, the gas sand produced high seismic amplitudes especially at far angles, the difference in AVA response due to increase in volume is minimal. It implies that the change in volume does not have significant impact on seismic amplitude change from the gas sand.

Constructive interference from tuning effect resulted to high seismic amplitudes. Gas sand reservoir produced higher seismic amplitudes despite that the acoustic impedance between the gas sand and encasing shale body revealed a minimal contrast. This signifies that the observed high seismic amplitude anomaly is as a result of the combined effect of both seismic amplitude response from gas sand and tuning effect. As a result of this, it is imperative not to assume that the presence of high seismic amplitude anomaly is significantly due to the presence of high volume of gas in the reservoir. A reservoir with thickness that is similar to the tuning thickness is expected to produce anomalous high seismic amplitude response due to the impact of both gas presence and tuning effect. It implies that thin brine saturated reservoir will produce high seismic amplitude anomaly due to tuning effect. This innovative approach revealed that to prevent drilling dry hole, it is expedient to analysis the presence of tunning effect in seismic amplitude responses in this field and in fields with similar geological

conditions so as to avoid drilling reservoirs mainly based on high seismic amplitude anomaly. This will help in managing seismic exploration plans and not to incur unnecessary financial exploration cost. The finding in this study may be further validated by the use of pre-stack seismic data which is not available at the time this study is conducted.

Acknowledgments

The authors appreciate Taadoy Geong Limited and Department of Petroleum resources for providing the data for this study. Also, Earth Signature Research Group (ESReG) and the Department of Geosciences, University of Lagos for their support in providing the computer workstation and the needed software for this work.

Disclosure statement

No potential conflict of interest was reported by the author(s).

References

∅degaard E, Avseth P. 2004. Well log and seismic data analysis using rock physics templates. First Break. 22 (10):37–43. doi: 10.3997/1365-2397.2004017.

Adeogba AA, McHargue TR, Graham SA. 2005. Transient fan architecture and depositional controls from near-surface 3-D seismic data, Niger Delta continental slope. Am Assoc Petroleum Geologists Bull. 89 (5):627–643. doi: 10.1306/11200404025.

Adeoti L, Adesanya OY, Oyedele KF, Afinotan IP, Adekanle A. 2017. Lithology and fluid prediction from simultaneous seismic inversion over Sandfish field, Niger Delta, Nigeria. Geosci J. 3(1):155–169. doi: 10.1007/s12303-017-0018-4.

Adeoti L, Allo OJ, Ayolabi EA, Akinmosin A, Oladele S, Oyeniran T, Ayuk MA. 2018. Reservoir fluid determination from angle stacked seismic volumes in 'Jay' field Niger Delta, Nigeria. J Appl Sci Environ Manag. 22 (4):453–458. doi: 10.4314/jasem.v22i4.2.

Adesanya OY, Adeoti L, Oyedele KF, Afinotan IP, Oyeniran T, Alli SA. 2021. Hydrocarbon reservoir delineation using simultaneous and elastic impedance inversions in a Niger Delta field. J Petroleum Exploration Prod Technol. 11 (7):2891–2904. doi: 10.1007/s13202-021-01191-5.

Allen J, Peddy C. 1994. Amplitude variation with offset: gulf coast case studies. Tulsa: Society of Exploration Geophysics. 10.1190/1.9781560802495.fm.

Allo OJ, Ayolabi EA, Adeoti L, Akinmosin A, Oladele S. 2022. Reservoir characterization for hydrocarbon detection using amplitude variation with angles constrained by localized rock physics template. J Afr Earth Sci. 192:104548. doi: 10.1016/j.jafrearsci.2022.104548.

Avseth P, Mukerji T, Mavko G. 2005. Quantitative seismic interpretation: applying rock physics tools to reduce interpretational risk. (UK): Cambridge University Press. 10.1029/2005EO400009.

Brown AR, Wright RM, Burkart KD, Abriel WL, McBeath RG. 1986. Tuning effects, lithological effects and depositional effects in the seismic response of gas reservoirs. Geophys Prospect. 34(5):623–647. doi: 10.1111/j.1365-2478.1986.tb00485.x.

Castagna JP, Swan HW. 1997. Principle of AVO crossploting. Leading Edge. 16(4):337–344. doi: 10.1190/1.1437626.

Chopra S, Castagna J, Portniaguine O. 2006. Seismic resolution and thin-bed reflectivity inversion. Can Soc Exploration Geophys Recorder. 31(1):19–25. doi: 10.1190/1.2369941.

Chung H, Lawton DC. 1999. A quantitative study of the effects of tuning on AVO effects for thin beds. Can J Exploration Geophy. 35:36–42. https://csegjournal.com/archives/1999-12/.

Cohen H, McClay K. 1995. Sedimentary and shale tectonics of the northwestern Niger delta front. Mar Petroleum Geol. 13(3):313–328. doi: 10.1016/0264-8172(95)00067-4.

Doust H, Omatsola E 1990. Niger delta. In: Edwards JD Santogrossi PA, editors. Divergent/Passive Margin Basins Vol. 48, Memoir AAPG: p. 201–338.

Evamy B, Haremboure J, Kamerling P, Knaap W, Molloy F, Rowlands P. 1978. Hydrocarbon habitat of tertiary Niger Delta. Am Assoc Petroleum Geologists Bull. 62:277–298. doi: 10.1306/C1EA47ED-16C9-11D7-8645000102C1865D.

Guo Q. 2014. Tunung, AVO, and flat spot effects in a seismic analysis of North Sea block F3 M.Sc. Thesis. (MI): Michigan Technological University.

Hamlyn W. 2014. Thin beds, tuning, and AVO. The leading edge 1394–1396. 10.1190/tle33121394.1.

Hilterman FJ. 2001. Seismic amplitude interpretation-distinguished instructor short course. Soc Exploration Geophysicists Eur Assoc Geoscientists Eng. doi: 10.1190/1.9781560801993.

Hussein M, Abu El-Ata A, El-Behiry M. 2020. AVO analysis aids in differentiation between false and true amplitude responses: a case study of El Mansoura Field, Onshore Nile Delta, Egypt. J Petroleum Exploration Prod Technol. 10(3):10.969–989. doi: 10.1007/s13202-019-00806-2.

Javaherian A, Salehi E, Pour MA, Farajkhah NK, Arabani MS. 2013. Quantitative seismic pre- stack analysis of potential gas-hydrate resources in the makran accretionary prism, offshore Iran. Mar Petroleum Geol. 48:160–170. doi: 10.1016/J.MARPETGEO.2013.07.015.

Kallweit RS, Wood LC. 1982. The limits of resolution of zero-phase wavelets. Geophysics. 47(7):1035–1046. doi: 10.1190/1.1441367.

Kamaci Z, Ciftci C. 2011. Amplitude versus offset (AVO) analysis modelling in hydrocarbon exploration: a case study. Int J Phys Sci. 6(4):908–916. doi: 10.5897/IJPS11.127.

Kim Y, Cheong S, Chun J, Cukur D, Kim S, Kim J, Kim B. 2020. Identification of shallow gas by seismic data and AVO processing: example of southwestern continental shelf of the Ulleung basin, East Sea, Korea. Mar Petroleum Geol. 117:104346. doi: 10.1016/j.marpetgeo.2020.104346.

Klett T, Ahlbrandt T, Schmoker J, Dolton G. 1997. Ranking of the world's oil and gas provinces by known petroleum volumes. U. S. Geological survey open-file report 97. http://pubs.er.usgs.gov/publication/ofr97463.

Kulke H. 1995. Nigeria. In: Tuttle M, Charpentier R Brownfield M, editors. The Niger Delta petroleum system: niger Delta Province, Nigeria, Cameroon, and Equatorial Guinea, Africa. USGS, Open File Report 99-50-H. https://pubs.usgs.gov/of/1999/ofr-99-0050/OF99-50H/OF99-50H.pdf.

Lambert-Aikhionbare DO, Ibe AC. 1984. Petroleum source bed generation of tertiary Niger Delta. American

Association of Petroleum Geologists Bulletin. 68(): 387–394. doi: https://doi.org/10.1306/AD460A2B-16F7-11D7-8645000102C1865D.

Marzec P, Pietsch K. 2012. Thin bedded strata and tuning effect as causes of seismic data anomalies in the top part of the Cenomanian sandstone in the Grobla-Rajsko-Rylowa area (Carplathian foreland, poland). Geological Q. 56(4):691–710. doi: 10.7306/gq.1050.

Mavko G, Murkeji T, Dvorkin J. 2003. The rock physics handbook. Cambridge: Cambridge University Press. 10.1017/CBO9780511626753.

Nanda NC. 2016. Seismic data interpretation and evaluation for hydrocarbon exploration and production 103–113. Switzerland: Springer international publishing. 10.100/978-3-319-26491-2_6.

Nwajide C. 2013. Geology of Nigeria's sedimentary basins. Lagos: CSS press 1–565.

Obaje NG, Wehner H, Schneeder G, Abubakar MB, Jauro A. 2004. Hydrocarbon prospectivity of Nigeria's inland basin. From the view point of organic geochemistry and organic petrology. Am Assoc Petroleum Geologists Bull. 88(3):325–353. doi: 10.1306/10210303022.

Ogbamikhumi A, Omorogieva OM. 2021. Rock property modelling and sensitivity analysis for hydrocarbon exploration in OSSY Field, Niger Delta Basin. J Petroleum Exploration Prod Technol. 11 (4):1809–1822. doi: 10.1007/s13202-021-01130-4.

Ostrander WJ. 1984. Plane wave reflection coefficients for gas sands at non-normal angles of incidence. Geophysics. 49(10):1637–1648. doi: 10.1190/1.1441571.

Osuntola OK. 1996. Amplitude variation with offset (AVO) analysis of some hydrocarbon bearing zones of the inner trend of the Niger Delta [Ph.D thesis]. Akure, Nigeria: Federal University of Technology.

Papageorgiou G, Chapman M. 2020. Seismic tuning of dispersive layers. Geophys Prospect. 69(3):622–628. doi: 10.1111/1365-2478.13009.

Ridwan TK, Hermana M, Lubis LA, Riyadi ZA. 2020. New AVO attributes and their applications for facies and hydrocarbon prediction: a case study from the northern Malay basin. Appl Sci. 10(21):7786–7803. doi: 10.3390/app10217786.

Roden R, Smith TA, Santogrossi P, Sacrey D, Jones G. 2017. Seismic interpretation below tuning with multiattribute analysis. Leading Edge. 36(4):330–339. doi: 10.1190/tle36040330.1.

Ross CP, Kinman DL. 1995. Non-bright spot AVO: two examples. Geophysics. 60(5):1398–1408. doi: 10.1190/1.1443875.

Russell B, Hampson D, Bankhead B. 2006. An inversion primer. Can Soc Exploration Geophys Recorder. 31 (10):101–108. https://csegrecorder.com/articles/view/an-inversion-primer.

Schlumberger. 2025. https://glossary.slb.com/en/terms/t/tuning_effect.

Short K, Stäuble A. 1967. Outline of geology of Niger Delta. Am Assoc Petroleum Geologists Bull. 51:761–779. doi: 10.1306/5D25C0CF-16C1-11D7-8645000102C1865D.

Shuey RT. 1985. A simplification of the Zoeppritz equations. Geophysics. 50(4):609–614. doi: 10.1190/1.1441936.

Simm R, Bacon M. 2014. Seismic amplitude. An interpreter's handbook. Cambridge University Press. 10.1017/CBO9780511984501.

Tuttle M, Charpentier R, Brownfield M. 1999. The Niger Delta petroleum system: niger Delta Province, Nigeria, Cameroon, and Equatorial Guinea, Africa. USGS, Open File Report 99-50-H. 10.3133/ofr9950H.

Uko ED, Emudianughe JE. 2014. AVO modelling of the South-East Niger Delta, Nigeria. J Geophys Remote Sens. 3(4):1–11. doi: 10.4172/2169-0049.1000131.

Weber KJ, Daukoru EM. 1975 Aug 25. Petroleum geological aspect of niger delta. Proceedings of the 9th World Petroleum Congress held in Houston; Texas (USA): Applied Science Publishers. p. 209–221.

Widess MB. 1973. How thin is a thin bed? Geophysics. 38 (6):1176–1180. doi: 10.1190/1.1440403.

Zoeppritz K. 1919. Erdbebenwellen VIIIB, Ueber reflexion and Durchgang seismischer Wellen durch Unstetigkeitsflaechen. Goettinger Nachr. I:66–84.